



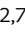




# Immune–epithelial cell cross-talk enhances antiviral responsiveness to SARS-CoV-2 in children

Vladimir G Magalhães<sup>1</sup> , Sören Lukassen<sup>2</sup>, Maike Drechsler<sup>1</sup>, Jennifer Loske<sup>3</sup>, Sandy S Burkart<sup>1,4</sup> , Sandra Wüst<sup>1</sup>, Eva-Maria Jacobsen<sup>5</sup> , Jobst Röhmel<sup>6</sup>, Marcus A Mall<sup>6,7,8</sup> , Klaus-Michael Debatin<sup>5</sup>, Roland Eils<sup>2,7,9</sup>, Stella Autenrieth<sup>10,11</sup> , Aleš Janda<sup>5</sup> , Irina Lehmann<sup>3,7</sup> & Marco Binder<sup>1,\*</sup> 

## Abstract

The risk of developing severe COVID-19 rises dramatically with age. Schoolchildren are significantly less likely than older people to die from SARS-CoV-2 infection, but the molecular mechanisms underlying this age-dependence are unknown. In primary infections, innate immunity is critical due to the lack of immune memory. Children, in particular, have a significantly stronger interferon response due to a primed state of their airway epithelium. In single-cell transcriptomes of nasal turbinates, we find increased frequencies of immune cells and stronger cytokine-mediated interactions with epithelial cells, resulting in increased epithelial expression of viral sensors (RIG-I, MDA5) via IRF1. *In vitro*, adolescent peripheral blood mononuclear cells produce more cytokines, priming A549 cells for stronger interferon responses to SARS-CoV-2. Taken together, our findings suggest that increased numbers of immune cells in the airways of children and enhanced cytokine-based interactions with epithelial cells tune the setpoint of the epithelial antiviral system. Our findings shed light on the molecular basis of children's remarkable resistance to COVID-19 and may suggest a novel concept for immunoprophylactic treatments.

**Keywords** age-dependence of disease; children; interferon response; RIG-I like receptors; SARS-CoV-2

**Subject Categories** Immunology; Microbiology, Virology & Host Pathogen Interaction; Molecular Biology of Disease

**DOI** 10.15252/embr.202357912 | Received 1 August 2023 | Revised 26 September 2023 | Accepted 28 September 2023 | Published online 11 October 2023

**EMBO Reports (2023) 24: e57912**

## Introduction

The COVID-19 pandemic represents one of the most devastating global health crises in modern times, with upwards of 6.9 million confirmed deaths (<http://covid19.who.int>, accessed July 10, 2023) and models suggesting a true death toll of up to 20 million or more (Wang *et al*, 2022). While severe, life-threatening COVID-19 chronic comorbidities such as hypertension, diabetes, cardiovascular disease, and obesity, as well as certain genetic factors, clearly play a role (Ng *et al*, 2021), the clearest and most striking predisposing factor is age. While only < 0.001% of school-age children died of the infection during the pandemic phase, infection fatality rates (IFR) increased almost perfectly exponentially with age reaching above 10% in the very elderly (O'Driscoll *et al*, 2021). This relation is also reflected in the general clinical features of infection, where children and adolescents generally display fewer symptoms with shorter duration as compared to adults and in particular the elderly, despite no strong difference in initial viral loads (Jones *et al*, 2021; Toh *et al*, 2022). The underlying molecular causes for this remarkable resistance of children and adolescents to develop severe COVID-19 have so far been incompletely understood.

In contrast to the situation with widely circulating respiratory viruses, such as influenza or respiratory syncytial virus (RSV), in the pandemic phase of SARS-CoV-2 individuals of all ages were immunologically naïve with no prior exposure to the virus. Hence, adaptive immune memory did not exist, and virus defense heavily relied on the responsiveness and strength of the innate immune system across all age groups. Indeed, hugely powered clinical association studies identified dysfunction of the antiviral type I interferon

1 Research Group "Dynamics of Early Viral Infection and the Innate Antiviral Response", Division Virus-Associated Carcinogenesis (F170), German Cancer Research Center (DKFZ), Heidelberg, Germany

2 Center for Digital Health, Berlin Institute of Health at the Charité - Universitätsmedizin Berlin, Berlin, Germany

3 Molecular Epidemiology Unit, Center for Digital Health, Berlin Institute of Health at the Charité - Universitätsmedizin Berlin, Berlin, Germany

4 Faculty of Biosciences, Heidelberg University, Heidelberg, Germany

5 Department of Pediatrics and Adolescent Medicine, Ulm University Medical Center, Ulm University, Ulm, Germany

6 Department of Pediatric Respiratory Medicine, Immunology and Critical Care Medicine, Charité - Universitätsmedizin Berlin, Corporate Member of Freie Universität Berlin and Humboldt-Universität zu Berlin, Berlin, Germany

7 German Center for Lung Research, Associated Partner, Berlin, Germany

8 Berlin Institute of Health at the Charité - Universitätsmedizin Berlin, Berlin, Germany

9 Health Data Science Unit, Faculty of Medicine, University of Heidelberg, Heidelberg, Germany

10 Research Group "Dendritic Cells in Infection and Cancer" (F171), German Cancer Research Center (DKFZ), Heidelberg, Germany

11 Department of Hematology, Oncology, Clinical Immunology and Rheumatology, University Hospital Tübingen, Eberhard Karls University Tübingen, Tübingen, Germany

\*Corresponding author. Tel: +49 6221 424974; E-mail: m.binder@dkfz.de

(IFN) system of the innate immune system to play a decisive role in the development of severe and life-threatening COVID-19 (Bastard *et al*, 2020; Zhang *et al*, 2020; Lopez *et al*, 2021). This was seemingly at odds with numerous early reports describing exuberant production of cytokines (“cytokine storm”), including type I IFNs, as a hallmark of severe COVID-19 (Lee *et al*, 2020; Lucas *et al*, 2020; Zhou *et al*, 2020). However, these seemingly disparate findings can be reconciled when the kinetics of the IFN response are taken into account (Park & Iwasaki, 2020; Wong & Perlman, 2022): Early and robust production of type I (and III) IFNs in the initially infected tissue of the upper respiratory tract is clearly antiviral and contributes to the immunological containment of the virus (Cheemarla *et al*, 2021; Lopez *et al*, 2021; Sposito *et al*, 2021), whereas a delayed onset but lasting induction of IFN rather represents a secondary production of IFNs as a consequence of dysregulated immune responses (cytokine storm) and is associated with more severe courses of the disease (Blanco-Melo *et al*, 2020; Lee *et al*, 2020; Lucas *et al*, 2020).

Early and local IFN is normally elicited intrinsically by virus-infected cells. Pattern recognition receptors (PRRs) of the host cell recognize nonself moieties, such as unusual nucleic acids introduced by the virus. Signaling downstream of the PRRs activates the transcription factors NFκB and IRF3, leading to the production and secretion of type I and III IFNs (see also Fig 1A). For RNA viruses, the RNA-sensing PRRs such as TLR3 and the RIG-I-like receptor (RLR) family, comprising RIG-I and MDA5 (with LGP2), are of particular relevance. SARS-CoV-2 is a positive-strand RNA virus that primarily infects ACE2-expressing ciliated epithelial cells in the lining of the respiratory tract (Lamers & Haagmans, 2022). Its ~30 kb genome encodes a highly efficient replicase complex, enabling rapid replication dynamics in permissive cells (Blanco-Melo *et al*, 2020; Chu *et al*, 2020b; Neufeldt *et al*, 2022). Additionally, numerous viral proteins possess the capacity to antagonize antiviral immune responses (Hayn *et al*, 2021; Lee *et al*, 2022). Taken together, the immediate-onset translation (positive-stranded RNA), rapid RNA replication, and high number of immune antagonists render SARS-CoV-2 highly efficient in preventing the mounting of host cell-intrinsic production of type I and III IFNs (Blanco-Melo *et al*, 2020; Neufeldt *et al*, 2022). This lack of IFN induction experimentally hampered the study of cellular sensing pathways, but recently MDA5 has been identified as the major sensor for SARS-CoV-2 in epithelial cells (Rebendenne *et al*, 2021; Sampaio *et al*, 2021; Yin *et al*, 2021). Interestingly, downstream of MDA5, viral antagonists specifically block the activation of IRF3 and thereby the induction of IFNs, while activation of NFκB remains possible, leading to the production of a pro-inflammatory set of cytokines (Neufeldt *et al*, 2022); in fact, NFκB has been reported to support SARS-CoV-2 replication (Nilsson-Payant *et al*, 2021). Very likely, this skewed cytokine profile directly contributes to the dysregulation of downstream events such as the recruiting and activation of professional immune cells mediating a proper antiviral immune response (classically termed type 1 immunity) (Wong & Perlman, 2022). Recently, we and others have found that, in contrast to the situation in adult patients, epithelial cells in the mucosa of children and adolescents more readily mount a robust IFN response upon SARS-CoV-2 infection (Loske *et al*, 2022; Yoshida *et al*, 2022). This is very likely a major contributor to the striking resilience of young individuals toward developing severe COVID-19.

In the present study, we aimed to better understand the underlying determinants for a proper induction of IFN in infected airway epithelial cells versus its failure. We previously observed a preactivated state of immune and epithelial cells in the upper airways of children prior to infection, characterized by a higher expression level of RLRs, in particular MDA5, as compared to adults (Loske *et al*, 2022). This sensitized state was associated with a rapid and robust induction of an IFN signature across epithelial and immune cell types upon SARS-CoV-2 infection. We hence speculate that subtle differences in the set-point of the virus-sensing machinery in epithelial cells would have a decisive role in the successful mounting of an IFN response. Confirming this hypothesis, we report that priming epithelial A549 cells with low to moderate doses of type I IFN or select inflammatory cytokines sensitizes their RLR pathway sufficiently to produce robust levels of type I and III IFNs upon SARS-CoV-2 infection. While MDA5 was the major sensor for this response, we additionally find a substantial contribution from RIG-I. With regard to why specifically children’s epithelial cells exhibit this primed state, we looked into the involvement of immune cells. In single-cell RNA sequencing (scRNA-Seq) data from nasal swabs taken from healthy children or adults, we found a substantially higher number of immune cells in the nasal mucosa of children, as well as substantially stronger immune-epithelial interactions (Loske *et al*, 2022). In an *in vitro* model, we could show that microbially stimulated immune cells (PBMC) of children are able to induce stronger RLR expression in A549 epithelial cells than PBMCs of adults, sufficient to enable robust IFN induction upon SARS-CoV-2 infection. This effect was mediated by both type I IFN as well as pro-inflammatory cytokines such as IFN-γ, IL-1β, and TNF. We confirmed these cytokines are constitutively expressed by immune cells in the nasal mucosa of children, very likely conferring the priming of their epithelial cells and eventually enabling the robust immune response to SARS-CoV-2 infection observed in children and adolescents.

## Results

### Priming with type I IFN renders lung epithelial cells competent to respond to SARS-CoV-2 infection

SARS-CoV-2 infection has been described to elicit a severely skewed cytokine response in epithelial cells, with a substantially dampened IFN component but high amounts of pro-inflammatory mediators (Blanco-Melo *et al*, 2020; Chu *et al*, 2020a; Lamers & Haagmans, 2022; Neufeldt *et al*, 2022) (for a scheme of the cell-intrinsic antiviral pathways relevant for this study, see Fig 1A). This lack of an early antiviral innate immune response at the site of primary infection is thought to be a major contributor to the development of severe COVID-19 (Yoshida *et al*, 2022). We and others have observed swifter and stronger IFN-responses upon SARS-CoV-2 infection in the upper airways of children than in those of adults (Neeland *et al*, 2021; Vono *et al*, 2021; Loske *et al*, 2022; Yoshida *et al*, 2022). In scRNA-Seq analyses, we found this to correlate with the presence of a subtle IFN-like transcriptional signature in nasal epithelial cells of children even in the absence of infection, with a clearly higher expression of genes of the viral sensing machinery such as RIG-I (encoded by the *RIGI* gene) and MDA5 (encoded by

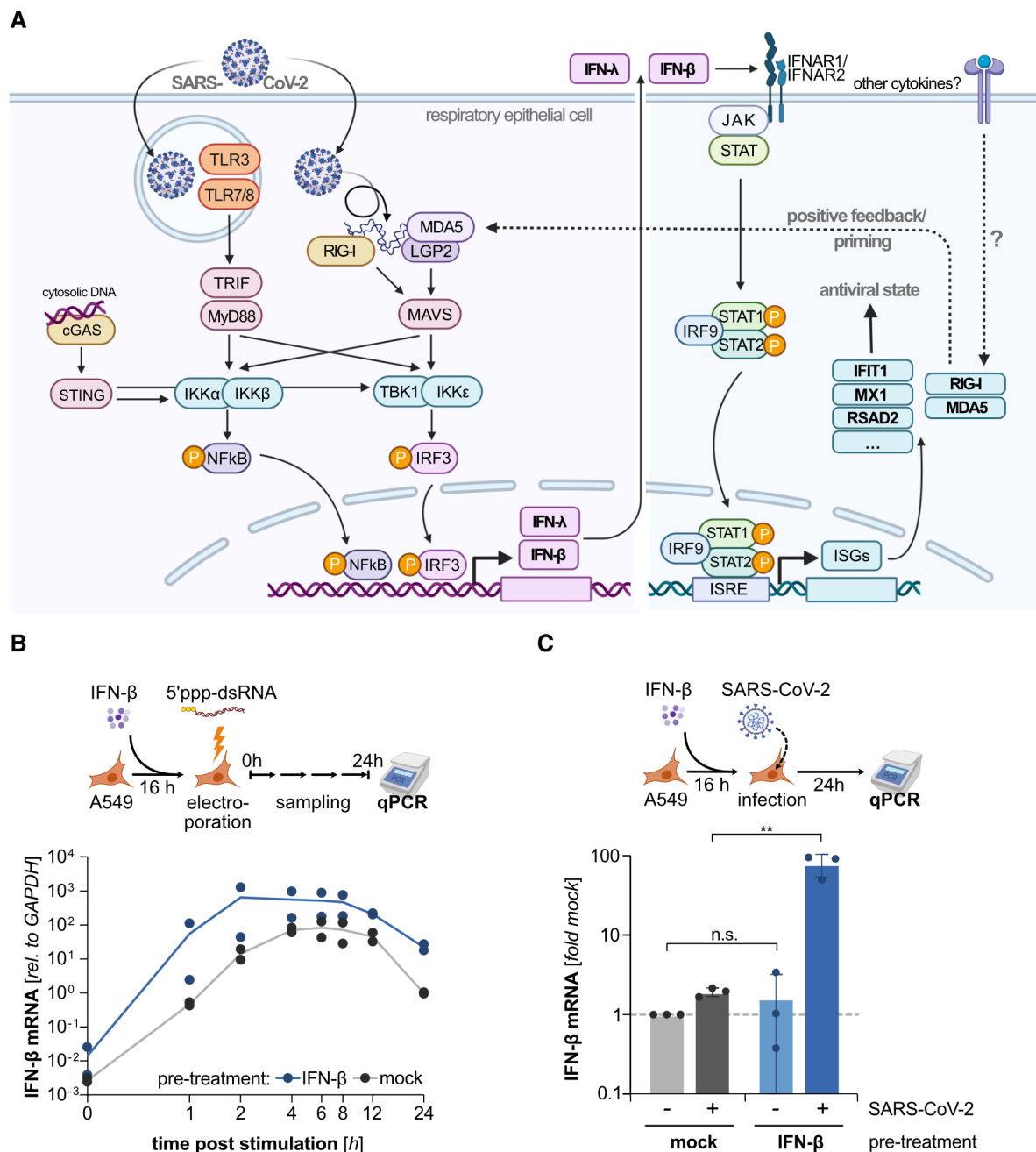


**Figure 1. Impact of cell priming on RLR signaling kinetics and interferon response to SARS-CoV-2 infection.**

**A** A schematic overview of the cell-intrinsic antiviral response pathways relevant to this study.

**B** A549 cells were mock-treated or primed with  $1 \times EC_{50}$  (170 IU/ml) of IFN- $\beta$  for 16 h. RIG-I was then synchronously stimulated in all cells by electro-transfection of 5'ppp-dsRNA. At the indicated time points, cells were lysed and analyzed for IFN- $\beta$  (*IFNB1*) gene expression by qRT-PCR. Biological replicates ( $n = 2$ ) are shown as individual dots.

**C** A549<sup>ACE2/TMPRSS2</sup> cells were mock-treated or primed as in (B), followed by infection with SARS-CoV-2 (MOI 0.1). At 24 h post infection, IFN- $\beta$  expression was measured by qRT-PCR. Values were normalized to 45S rRNA levels and expressed relative to non-infected mock-treated cells. Bars represent means  $\pm$  SD,  $n = 3$  (biological replicates, individual experiments shown as dots). Statistical significance between the corresponding uninfected and infected samples was tested by an unpaired two-tailed  $t$ -test; \*\* $P < 0.01$ .

Source data are available online for this figure.

the *IFIH1* gene) (Loske *et al.*, 2022). This suggested a primed state of epithelial cells in children, which might render their innate antiviral system more sensitive in detection and more robust in its response.

To confirm this hypothesis, we *in vitro* primed A549 human lung epithelial cells and assessed the effect on their antiviral response dynamics. We primed the cells by pretreating them overnight (16 h) with a moderate dose of 170 IU/ml of IFN- $\beta$ , determined to be the EC<sub>50</sub> with regard to ISG induction in A549 cells (Fig EV1A). We then triggered RLR-signaling by electro-transfection of the RIG-I agonist 5'ppp-dsRNA, as described in Burkart *et al.* (Burkart *et al.*, 2023). To monitor RLR pathway activity over time, we measured IFN- $\beta$  (encoded by the *IFNB1* gene) transcription as a specific downstream readout for antiviral PRR signaling. In non-pretreated cells, dsRNA stimulation gradually induced IFN- $\beta$  expression, reaching maximum levels at 4–8 h and declining thereafter (Fig 1B, gray line). As expected, pretreatment alone only triggered negligible IFN- $\beta$  transcription (Fig 1B, 0 h and Fig 1C, mock-infected; note that baseline expression of IFN- $\beta$  is virtually absent with c<sub>T</sub> values close to the detection limit). However, upon dsRNA stimulation, IFN- $\beta$  primed cells mounted a 1–2 log stronger response than non-pretreated cells (Fig 1B, blue line). This response was not only higher in amplitude but also notably swifter, reaching peak activation already at 2 h after stimulation. This illustrated the quantitative but also qualitative enhancement of RLR signaling and IFN induction in cells with a primed antiviral system.

While priming cells with IFN is not a novel concept, we propose that in particular this kinetic impact—often neglected in previous studies—will provide a significant advantage for cells in responding to and fending off virus infection. Many viruses, and in particular SARS-CoV-2, encode and express antagonists of the cellular antiviral defense (Lee *et al.*, 2022). We and others have described SARS-CoV-2 to potentially suppress the induction of IFNs in respiratory epithelial cells, likely due to its rapid replication and expression of a multitude of antagonists (Lee *et al.*, 2022; Neufeldt *et al.*, 2022; Thorne *et al.*, 2022). We hypothesize that upon priming, the faster response dynamics of the antiviral system could confer a substantial advantage (“head-start”) to cells, such that the IFN system could be elicited before viral antagonism is fully mounted. To test this hypothesis, we pretreated A549 cells expressing ACE2 and TMPRSS2 (A549<sup>ACE2/TMPRSS2</sup>) with the same regimen of 1× EC<sub>50</sub> of IFN- $\beta$  for 16 h and then infected them with SARS-CoV-2. As described previously, SARS-CoV-2 infection did not elicit an IFN- $\beta$  response in mock-treated A549 cells (Fig 1C, gray bars). In contrast, IFN-priming of cells restored their capacity to mount a robust response upon SARS-CoV-2 infection with ~100-fold induction of IFNB1 transcripts (Fig 1C, blue bars). We confirmed these observations also in another human lung epithelial cell line, Calu-3, in which IFN levels ensuing SARS-CoV-2 infection were also increased upon prior priming (Fig EV1B). Taken together, this demonstrates that priming of epithelial cells can qualitatively change their response to virus infection. Mimicking the situation in adult patients, untreated A549 cells fail to induce an IFN response upon SARS-CoV-2 infection. However, upon priming, similar to the situation observed in children, A549 cells become sensitized and able to rapidly respond to virus infection. This strongly suggests that also *in vivo* tissue exposure to cytokines can critically modulate the responsiveness of epithelial cells to SARS-CoV-2.

## Primed epithelial cells mount an effective antiviral state upon SARS-CoV-2 infection through viral sensing by MDA5 and RIG-I

Having established primed versus nonprimed A549 cells as a simplistic model of the different states of the nasal epithelium in children versus adults, we next addressed two important questions: (i) which PRR(s) detect SARS-CoV-2 in epithelial cells? and (ii) is the IFN response elicited upon infection of primed cells antiviral? Previous studies pinpointed MDA5 as the major cytosolic sensor for SARS-CoV-2 (Rebendenne *et al.*, 2021; Sampaio *et al.*, 2021; Thorne *et al.*, 2021; Yin *et al.*, 2021), but TLRs have also been implicated in cytokine responses to the virus (Asano *et al.*, 2021; Khanmohammadi & Rezaei, 2021). We, therefore, made use of A549 cells with CRISPR/Cas9-based functional knockouts (KO) of the central adaptors of different PRR axes: MyD88 and TRIF for the TLRs, STING for cytosolic DNA sensors such as cGAS, and MAVS for the RLRs RIG-I and MDA5 (see Fig 1A for a schematic overview); IFNAR<sup>KO</sup> cells were used as a negative control incapable of being primed by IFN- $\beta$ . We observed that only cells devoid of MAVS entirely abrogated IFN- $\beta$  induction, while KO of STING, MyD88, or TRIF had no effect (Fig 2A). To identify the actually responsible receptor upstream of MAVS, we investigated the role of RIG-I and MDA5 individually by priming individual KOs and double KO cell lines and assessing their IFN response upon infection. Since MDA5 and RIG-I are classical ISGs themselves, pretreatment of cells with IFN- $\beta$  resulted in high MDA5 and RIG-I protein levels (Figs EV1C and 2C, compare NT and IFNAR<sup>KO</sup>). SARS-CoV-2 infection of primed cells lacking RIG-I but expressing high levels of MDA5 exhibited strong IFN- $\beta$  induction similar to or even slightly stronger than wild-type (NT) cells (Fig 2B). In contrast, the absence of MDA5, despite high levels of RIG-I, resulted in a 2.4-fold reduction of IFNB1 transcripts relative to control cells. Strikingly, IFN- $\beta$  induction was fully abolished when both sensors were lacking (Fig 2B), suggesting that both RIG-I and MDA5 are essential for a full-fledged IFN response in epithelial cells. This was also confirmed at a level downstream of IFN production and IFN receptor signaling by monitoring the phosphorylation of STAT2. Activation of STAT2 was still observed upon infection of RIG-I or MDA5 single KOs, but was fully diminished only in the double KO cells (Figs 2C and EV1D). Hence, priming of cells with IFN allowed us to study SARS-CoV-2 sensing pathways at the endogenous level (i.e., without requiring ectopic expression of PRRs) and to genetically dissect the molecular requirements. We identified a co-requirement of MDA5 and RIG-I for mounting a full-fledged IFN response.

While our data clearly showed the restoration of an RLR-mediated IFN response toward SARS-CoV-2 infection in IFN- $\beta$ -primed cells, it remained unclear whether this response was effectively antiviral. Therefore, we next assessed viral replication upon infection of IFN- $\beta$ -primed cells. We again used a low dose (1× IC<sub>50</sub>) of IFN- $\beta$  for pretreatment of A549<sup>ACE2/TMPRSS2</sup> cells and then infected them with SARS-CoV-2. As expected, viral replication at 24 h postinfection was significantly (~10-fold) reduced in IFN-pretreated cells as compared to mock-treated cells (Fig 2D, brown bars), while no effect was observed in IFNAR<sup>KO</sup> control cells (Fig 2D, green bars). Strikingly, IFN- $\beta$ -pretreatment tended to be less effective in suppressing viral replication in cells lacking functional MDA5 or RIG-I and was almost completely ineffective (no statistically significant effect) in RIG-I/MDA5<sup>DKO</sup> cells lacking both

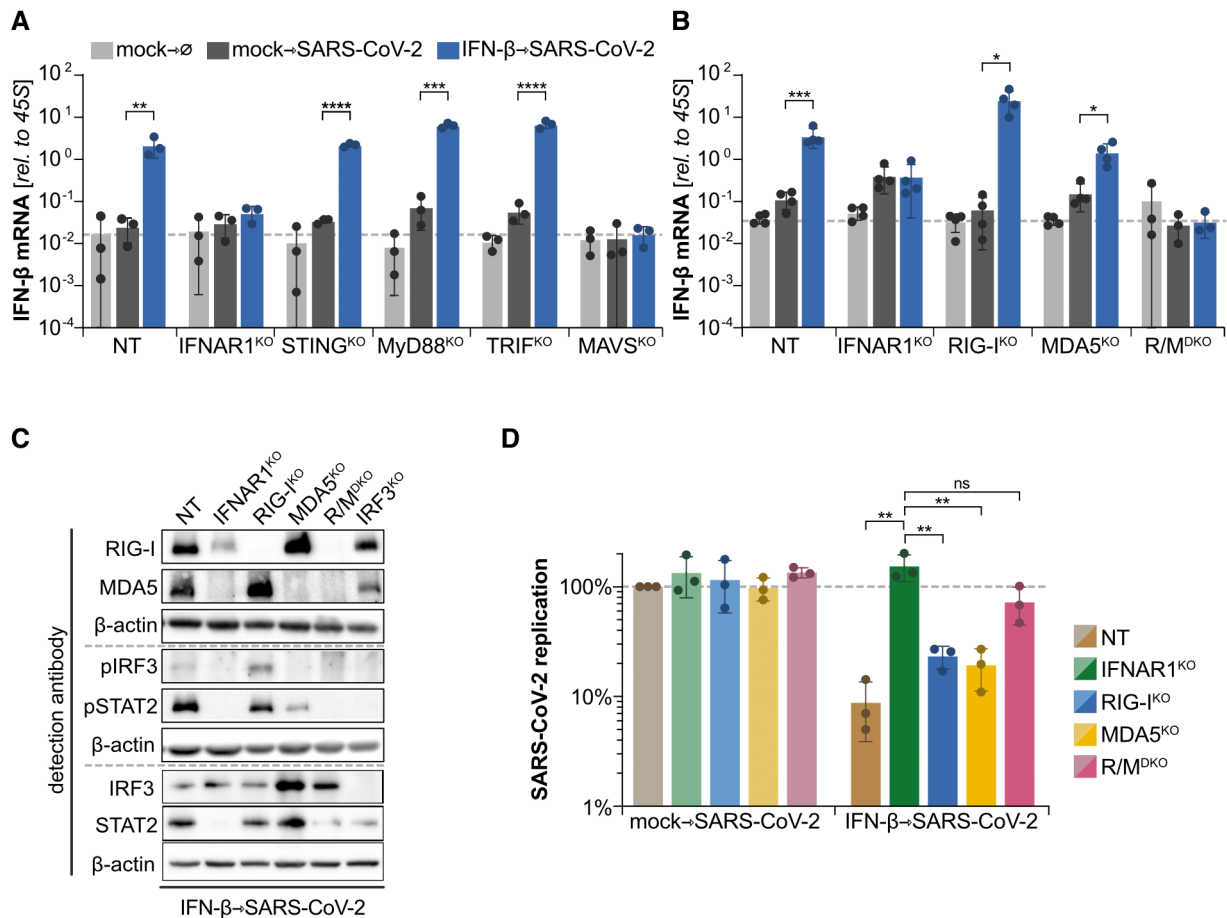


**Figure 2. PRR-dependence of the antiviral response to SARS-CoV-2 in primed cells.**

**A, B** A549<sup>ACE2/TMPRSS2</sup> cells harboring the indicated CRISPR/Cas9-mediated functional KOs of (A) the major PRR adaptors or of (B) the RLRs (R/M<sup>DKO</sup>: RIG-I/MDA5 double-KO) were either mock-treated or primed with IFN-β followed by infection with SARS-CoV-2 (MOI of 0.1) for 24 h. IFN-β (*IFNB1*) gene expression was determined by qRT-PCR. Values were normalized to 45S rRNA levels.

**C** Primed and infected A549<sup>ACE2/TMPRSS2</sup> cells (as in A, B above) with the indicated KOs were lysed 24 h post infection and analyzed by immunoblotting using the indicated antibodies. The blot is representative of two biological replicates.

**D** Mock-treated or primed cells with the indicated KOs were infected with SARS-CoV-2 (MOI 0.1). At 24 h postinfection, intracellular viral genome levels were determined by qRT-PCR. Values were normalized to 45S rRNA levels and expressed relative to nonprimed wild-type (NT) cells.

Data information: In (A, B and D), bars represent mean ± SD, *n* = 3 (biological replicates, individual experiments shown as dots). Statistical significance in (A and B) was tested between mock uninfected and infected samples, and between mock infected and IFN-β-primed infected samples by an unpaired two-tailed *t*-test; in (D) significance was tested by an unpaired one-tailed *t*-test, comparing each sample against the respective IFNAR1<sup>KO</sup> control. \**P* < 0.05, \*\**P* < 0.01, \*\*\**P* < 0.001, \*\*\*\**P* < 0.0001, no asterisk: not significant.

Source data are available online for this figure.

receptors (Fig 2D, pink bars). This was surprising, as generally the direct induction of ISGs downstream of IFN receptor signaling was held accountable for the antiviral effects of IFN-(pre-)treatment. Our results now underscore the critical importance of RLR-mediated positive feedback for the effects of low-dose IFN. Indeed, at higher doses of IFN-β (10× IC<sub>50</sub>) the effects of pretreatment were significantly stronger and virtually independent of the presence of RLR feedback (Fig EV1E). These observations, therefore, demonstrate a clear antiviral effect of the cell-intrinsically induced IFN response upon RLR-mediated recognition of the SARS-CoV-2. Moreover, they support the notion that low local concentrations of IFNs in the tissue can effectively prime cells for more sensitive detection of potential viral infection, rather than directly eliciting an antiviral state.

### Elevated levels of MDA5 and RIG-I in epithelial cells of children suffice to induce IFN production upon SARS-CoV-2 infection

The above experiments suggested that IFN-priming of cells increases the sensitivity of the antiviral system largely by inducing the expression of viral sensors. Nonetheless, IFN-treatment upregulates a plethora of genes, possibly also factors downstream of the RLRs. In order to assess if the enhanced expression of only RIG-I or MDA5 suffices to reconstitute productive viral sensing, we generated stably overexpressing cells. We reconstituted RIG-I or MDA5 expression in double KO cells (A549 RIG-I/MDA5<sup>DKO</sup>) by lentiviral transduction under the control of the weak ROSA26 promoter (Fig 3A, bottom). This led to the expression of moderate amounts of either RIG-I or



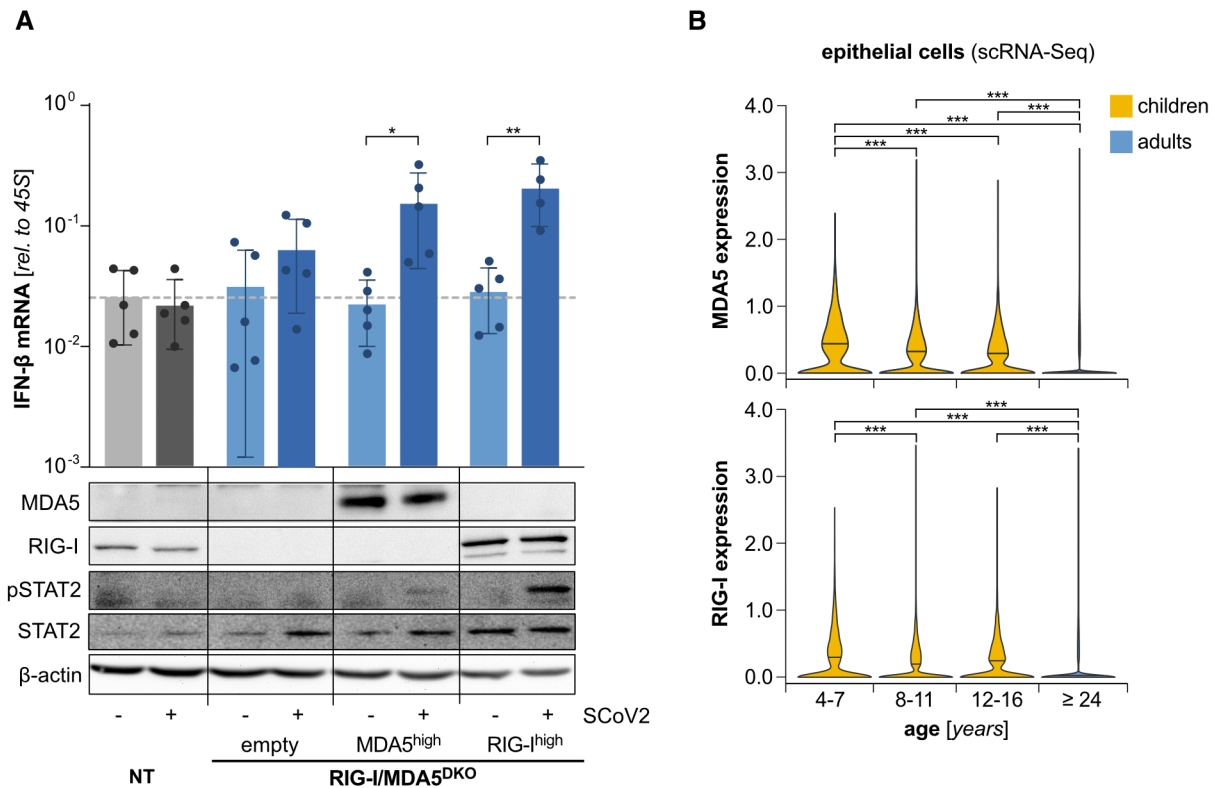


**Figure 3. Impact of increased RLR expression on the antiviral response to SARS-CoV-2 in nonprimed cells.**

**A** A549<sup>ACE2/TMPRSS2</sup> cells deficient for RIG-I and MDA5 were reconstituted to express only MDA5 or RIG-I by lentiviral transduction. Cells were mock-infected or infected with SARS-CoV-2 (upper panel: MOI 0.01, lower panel: MOI 1) for 24 h. IFN- $\beta$  (*IFNB1*) expression was determined by qRT-PCR (bar graph), and MDA5, RIG-I, and STAT2 protein levels as well as STAT2 phosphorylation (pSTAT2) were analyzed by immunoblotting (lower panel). qPCR values were normalized to 45S rRNA and expressed as mean  $\pm$  SD,  $n \geq 4$  (biological replicates, individual experiments shown as dots). Statistical significance between mock and infected samples was tested by a paired two-tailed t-test. \* $P < 0.05$ , \*\* $P < 0.01$ , no asterisk: not significant. Immunoblot representative of two biological replicates.

**B** Nasal swabs were taken from healthy individuals of the indicated age groups ( $n = 18$  children,  $n = 23$  adults) and analyzed by scRNA-Seq (Loske et al, 2022). MDA5 (*IFIH1*) and RIG-I (*RIGI*) gene expression were quantified across all epithelial cell types of children and adults and displayed as violin plots (median indicated). Statistical significance between all conditions was tested using a two-tailed Wilcoxon comparison adjusted with a Bonferroni correction. \*\*\* $P < 0.001$ , no asterisk: not significant.

Source data are available online for this figure.

MDA5 without triggering signaling and IFN induction on its own (Fig 3A, light bars). Upon infection with SARS-CoV-2, however, IFNB1 transcription was significantly induced both in RIG-I and MDA5 overexpressing cells (Fig 3A, dark bars). These experiments demonstrate that, indeed, the enhanced expression of RLRs suffices to sensitize cells and enable them to mount an IFN response toward SARS-CoV-2 despite its fast replication and strong immune antagonism.

This corroborates our previous observation that higher expression of viral sensors in the nasal airways of children prior to infection is associated with significantly stronger IFN responses upon SARS-CoV-2 infection (Loske et al, 2022). Briefly, in that earlier study, we analyzed nasal airway swabs of healthy and SARS-CoV-2-infected children and adults by scRNA-Seq. Now focusing exclusively on the samples of healthy donors, comprising 18 children (4–16 years, median age 9.0) and 23 adults (24–77 years, median age 46.0), finer analysis of the data revealed a gradual decrease of MDA5 expression levels in nasal epithelial cells with increasing age

of the individuals (Fig 3B). RIG-I was also confirmed to be significantly higher expressed in the epithelium of children and adolescents; however, the gradual decrease between age groups was less clear (Fig 3B).

Taken together, our data from A549 cells shows the efficacy of IFN-priming to be largely mediated by the induced expression of the viral sensors themselves, RIG-I and MDA5. Coherently, we find age-dependent expression levels for MDA5 and RIG-I in nasal airway samples of healthy volunteers, corroborating the notion of functional priming of epithelial cells in children and teenagers.

#### Nasal mucosa of children exhibits higher number of immune cells and substantially more immune-epithelial cell interactions

Having established the molecular functioning of the increased cellular responsiveness to SARS-CoV-2 infection in primed epithelial cells, we next wanted to understand the upstream source of this priming in the nasal airways of children. We hypothesized that

tissue resident and other local immune cells in the mucosa may be involved in the priming of epithelial cells and modulating the homeostatic set-point of cell-intrinsic immunity in the tissue, as has been suggested before (Larsen *et al*, 2020; Hewitt & Lloyd, 2021). Therefore, we again turned to the scRNA-Seq data of nasal swabs of healthy children and adults. First, we assessed the number of immune cells present in the mucosal samples. We found vastly higher proportions of immune cells in the nasal mucosa of children (> 50%) than that of adults (< 10%), in particular neutrophils, T-cells, macrophages, and dendritic cells (Fig 4A, finer subtyping of cells in Fig EV2A) (Loske *et al*, 2022). This supported the notion that immune cells may indeed play an important role in priming the airway epithelium in children. To further corroborate this notion, we then analyzed immune–epithelial cell interactions. For this purpose, we mapped the expression levels of ligands (e.g., cytokines) and their corresponding receptors at the single cell level using the Cell-Chat database (Jin *et al*, 2021), which we augmented with a recently published very comprehensive interaction map (“physical wiring diagram”) of the human immune system (Shilts *et al*, 2022). This method allowed us to infer possible molecular interactions of each cell type with every other cell type in the sample and to quantify both the number of detected ligand–receptor pairs between two interacting cell types as well as their interaction strength by taking expression levels into account. Strikingly, we observed substantially more but also stronger inferred immune–epithelial cell interactions in children than in adults (Fig 4B bar graph, Fig EV2B and C). In the circular interaction plot of Fig 4B, each immune cell type is connected to the epithelial cell types it can interact with. If the number of distinct ligand–receptor pairs of such an interaction is higher in children than in adults, the arrow is yellow; if adults expressed more ligand–receptor pairs, the arrow is blue. This clearly showed that all immune cell interactions (except for those of proliferating T-cells) were based on a broader set of ligand–receptor pairs in children than in adults, fostering the notion of a substantially higher connectivity of immune and epithelial cells in the mucosa of younger individuals.

#### Immune cells stimulate RLR expression in epithelial cells in an IFN-dependent as well as -independent manner

Based on the above analyses, we speculated that the increased presence of immune cells in the nonsterile environment of the nasal mucosa may shape the local cytokine milieu and could be decisive for the heightened expression of RIG-I and MDA5. In order to approach this in a simplified *in vitro* experimental model, we used isolated human immune cells (peripheral blood mononuclear cells, PBMC) and mimicked microbial encounters by exposing them to a Gram-negative model bacterium (*Yersinia enterocolitica*, Ye) (Fig 4C). To prevent bacterial overgrowth, bacteria were killed after 1 h by gentamicin. In order to functionally assess the ensuing cytokine response, we transferred the sterile-filtered PBMC supernatant to A549 cells 24 h later. We observed a substantial increase in expression of both RLRs in A549 cells exposed to the supernatants of stimulated PBMCs (Figs 4D and EV2D). As RIG-I and MDA5 are ISGs, this induction was likely to be mediated by IFNs produced by innate immune cells. Indeed, KO of the type I IFN receptor (IFNAR<sup>KO</sup>) in A549 cells dampened RLR induction significantly, and the additional KO of type II and III IFN receptors (IFN<sup>TRKO</sup>) further

reduced it (Fig 4D). Unexpectedly, however, even in the absence of all three classes of IFN receptors, both RIG-I and MDA5 levels were still significantly induced. We, therefore, analyzed the PBMC supernatants for their cytokine content. As expected, Ye-exposed PBMCs secreted substantial amounts of type I ( $-\alpha 2$ ,  $-\beta$ ) and II ( $-\gamma$ ) IFNs (Fig 4E), coherent with the reduced RLR induction in IFN receptor KO cells. We further detected the secretion of several pro- and anti-inflammatory cytokines, in particular IL-1 $\beta$ , IL-6, IL-10, and TNF, some or all of which may contribute to the observed RLR induction (Fig 4E). In order to compare these *in vitro* findings to the physiological situation, we specifically analyzed the immune cell population from the nasal mucosa of healthy children and adults for their expression of these cytokines, incl. IFN- $\gamma$  as a common inflammatory mediator. Strikingly, we found significantly higher expression for IFN- $\gamma$ , IL-6, IL-10, and TNF (but not IL-1 $\beta$ ) in healthy children as compared to adults (Fig 4F), resembling and confirming our *in vitro* observations. To further understand the source of these cytokines and their contribution to immune–epithelial communication *in vivo*, we analyzed ligand–receptor interactions of the single cell data specifically for IFN- $\gamma$  and TNF (Fig 4G) as well as IL-1 and IL-10 (Fig EV2E–H); there was no significant ligand–receptor interaction of IL-6. Indeed, all four analyzed cytokines exhibited notably higher connectivity to the epithelial cell compartment, both in terms of the number of interactions as well as the respective information flow, that is, the interaction strength (Fig EV2C). Interestingly, IL17A<sup>+</sup> T-cells appeared to be major producers of IFN- $\gamma$ , TNF, and IL-10 in children, as well as proliferating NK cells for IFN- $\gamma$  and macrophages for IL-1 (Figs 4G and EV2E–H).

In summary, stimulation of PBMCs *in vitro* led to the secretion of type I IFNs as well as pro- and anti-inflammatory cytokines such as IFN- $\gamma$ , TNF, IL-1 $\beta$ , IL-6, and IL-10. These secreted cytokines mediated upregulation of RIG-I and MDA5 in epithelial cells, to a certain degree even in the absence of IFN receptors. Particularly, IFN- $\gamma$ , TNF, IL-6, and IL-10 were also found to be elevated (at the mRNA level) in the mucosal immune cells of children and to be involved in immune–epithelial cell interactions. This supports the hypothesis that immune cells in the mucosa of healthy children are required to prime the antiviral system of epithelial cells.

#### IFN-independent priming induces sufficient MDA5 and RIG-I expression to respond to SARS-CoV-2

We observed enhanced immune–epithelial cross-talk in the mucosa of children and immune cell-derived cytokines beyond type I and II IFNs to be capable of stimulating the expression of MDA5 and RIG-I in epithelial cells. To further test which (if any) of the above-identified cytokines have the potential to induce RLR expression, we treated A549 lung epithelial cells with recombinant IFN- $\gamma$ , IL-1 $\beta$ , IL-6, IL-10, or TNF at a concentration of 10 ng/ml, comparable to the amount measured in the supernatants of activated PBMCs (compare Fig 4E). Eight hours after stimulation, we measured MDA5 and RIG-I levels by qRT-PCR and Western blotting and found particularly IFN- $\gamma$  and TNF, and to a lesser extent IL-1 $\beta$ , to induce MDA5 and RIG-I expression (Figs 5A and EV3A). As to be expected, IFN- $\gamma$  required the presence of the IFN- $\gamma$ -receptor (IFNGR), and RLR induction was abolished in IFN<sup>TRKO</sup> (but not IFNAR<sup>KO</sup>) cells. In contrast, the effects of TNF and IL-1 $\beta$  were fully independent of any IFN-signaling (Figs 5A and EV3A). IL-6 and IL-10 did not affect RLR

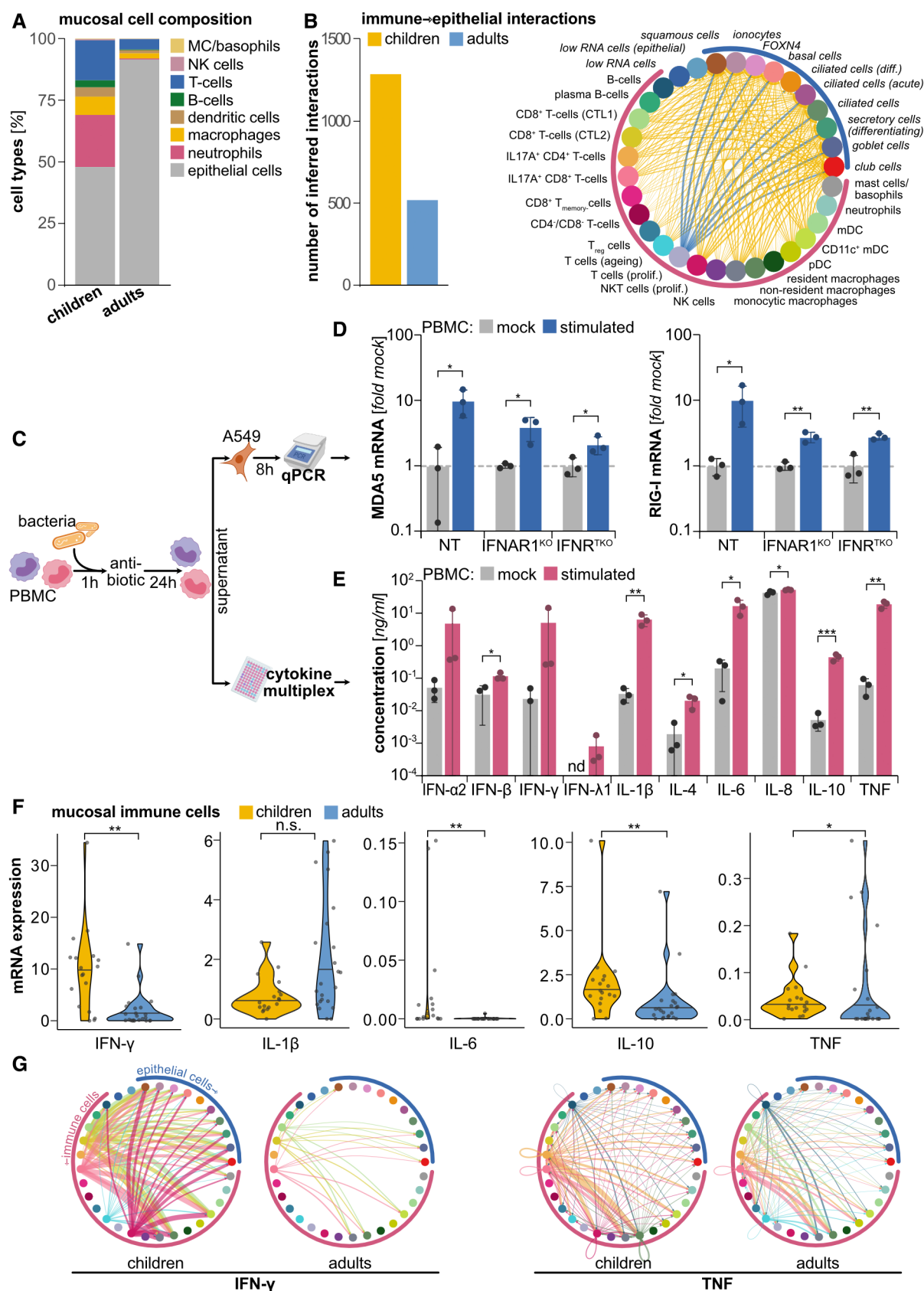


Figure 4.



**Figure 4. Antiviral priming of epithelial cells by immune–epithelial cell crosstalk through cytokines.**

scRNA-Seq of nasal swabs from healthy children (4–16 years,  $n = 18$ ) and adults ( $\geq 24$  years,  $n = 23$ ) (Loske et al, 2022).

- A Assignment of single cell types and states based on their transcriptional profile (Loske et al, 2022). Similar types were grouped into more general classes (“epithelial cells,” “T-cells”). The relative abundance of immune cell types was determined and compared between children and adults. Figure EV3A shows a detailed immune cell composition.
- B Cell interactivity was determined in children and adults based on the expression of corresponding pairs of signaling ligands (on immune cells) and receptors (on epithelial cells). The bar graph (left) shows the total number of inferred interactions. The interaction plot (right) shows interactions between specific immune and epithelial cell types. Line thickness indicates the number of ligand–receptor interactions (yellow = higher numbers in children, blue = in adults). Outer circle segments: blue marks epithelial cells, pink immune cells. See also Fig EV3B.
- C Isolated human PBMCs were exposed to live Gram-negative bacteria (*Yersinia enterocolitica*, Ye), killed after 1 h by gentamicin treatment. Upon further incubation for 24 h, culture supernatants were harvested and analyzed.
- D A549 NT (wild-type control), IFNAR1<sup>KO</sup> and type I, II, III and IFN receptor triple KO (IFNR<sup>TKO</sup>) were incubated with collected PBMC supernatants for 8 h. Expression levels of MDA5 (*IFIH1*) and RIG-I (*RIGI*) were determined by qRT-PCR. Values were normalized to GAPDH levels and expressed relative to wild-type A549 incubated with supernatants from mock-stimulated PBMC.
- E The cytokine content of the supernatants of mock-treated or Ye-exposed PBMCs was analyzed by an electroluminescent multiplex assay.
- F ScRNA-Seq data (see A) were analyzed for the expression of cytokines (see E) across all immune cell types and states. Values displayed as violin plots with the average per cell expression level of each donor ( $n = 18$  children,  $n = 23$  adults) shown as dots.
- G ScRNA-Seq data were analyzed for ligand–receptor interactions between cell types (cell type identified by color; see panel B) specifically for IFN- $\gamma$  (left) and TNF (right) signaling in children and adult samples. Interaction strength is coded by line thickness; direction (ligand→receptor) indicated by arrowheads; arrows are color-coded by cell type of origin. See also Fig EV3.

Data information: In (D and E) bars represent means  $\pm$  SD,  $n = 3$  (biological replicates, individual experiments shown as dots). The statistical significance between mock and stimulated samples was tested by an unpaired, one-tailed t-test. \* $P < 0.05$ , \*\* $P < 0.01$ , \*\*\* $P < 0.001$ , no asterisk: not significant. In (F) statistical significance was tested using the Kolmogorov–Smirnov test with a Benjamini–Hochberg correction. \*\* $P < 0.01$ , \* $P < 0.05$ .

Source data are available online for this figure.

expression in A549 cells at all. Importantly, these experiments demonstrated that cytokines such as IFN- $\gamma$ , TNF, and IL-1 $\beta$  produced by immune cells *in vitro* and detected *in vivo* in the mucosa of healthy children are capable of functionally priming epithelial cells to induce the expression of viral sensors.

We next investigated how these cytokines might upregulate RLRs, which clearly are not among their canonical target genes. TNF and IL-1 $\beta$  are hallmark pro-inflammatory cytokines. Recently, they were described as being capable of indirectly inducing ISG expression via the release of mitochondrial DNA, which then activates the cytosolic cGAS-STING-IRF3 pathway leading to the production of type I IFN (Aarreberg et al, 2019; Willemssen et al, 2021). While secreted IFN was dispensable for RLR induction by TNF and IL-1 $\beta$  in our experiments (Fig 4G), direct induction downstream of cGAS and STING was still plausible. Therefore, we checked MDA5 and RIG-I expression in TNF- or IL-1 $\beta$ -stimulated STING<sup>KO</sup> and IRF3<sup>KO</sup> cells. Surprisingly, at 8 h poststimulation, both STING and IRF3-deficient cells induced RLR transcription to comparable levels as WT cells, suggesting that early RLR induction occurred independently of the cGAS-STING axis (Figs 5B and EV3B). Another important transcription factor of the IRF family is IRF1. Recently, IRF1 was described as being involved in the constitutive expression of antiviral genes such as TLR2, TLR3, and OAS2 (Panda et al, 2019) and contributing to TNF- and IL-1 $\beta$ -mediated ISG expression in monocytes and epithelial cells (Yarilina et al, 2008; Aarreberg et al, 2019). In fact, in IRF1<sup>KO</sup> cells, we observed virtually no induction of RIG-I and MDA5 transcripts upon IL-1 $\beta$  treatment, and also TNF-induced expression was clearly reduced (Figs 5B and EV3B). Notably, IRF1 is also an important and well-established transcription factor in the IFN- $\gamma$  response (Lee et al, 2006; Murtas et al, 2013; Forero et al, 2019). We furthermore found elevated IRF1 expression in almost all epithelial and many immune cell types in the nasal mucosa of children as compared to adults (Fig EV3C). Taken together, from the cytokines identified *in vitro* and *in vivo*,

we found TNF, IFN- $\gamma$ , and, to a lesser extent, IL-1 $\beta$  to be capable of stimulating the expression of RIG-I and MDA5 in A549 epithelial cells. This suggests those cytokines critically determine homeostatic expression of the antiviral system in the epithelium, particularly in children, with IRF1 being the central transcriptional regulator.

Both *in vitro* and *in vivo*, IL-1 $\beta$  appeared to play a minor role. IFN- $\gamma$  is antiviral, and its signaling and transcriptional responses have significant overlap with type I/III IFN, hence, its function in the priming of cells likely resembles that of IFN- $\beta$  (Figs 1 and 2). TNF, on the other hand, is a highly pleiotropic cytokine involved in organogenesis tissue homeostasis, and, importantly, it is a critical mediator of inflammatory responses. Its biological activity is highly context- and likely concentration-dependent. We therefore further investigated the capacity of IFN-independent priming of epithelial cells by TNF. Confirming our above finding of IRF1-dependence, TNF-treatment induced transcription of IRF1 to higher levels than IFN- $\beta$ , whereas the classical type I ISG Mx1 was substantially higher in IFN-treatment (Fig 5C). The RLRs MDA5 and RIG-I, however, were induced similarly by both cytokines. We next assessed MDA5 expression at the protein level upon different TNF doses and treatment times. Indeed, protein levels increased in a dose- and time-dependent manner (Fig 5D). We then pretreated A549<sup>ACE2/TMPRSS2</sup> cells with increasing TNF doses for 8 h before infecting them with SARS-CoV-2. Twenty-four hours postinfection, we then analyzed the ensuing antiviral response by measuring IFN- $\beta$  mRNA levels. While TNF pretreatment alone did not induce IFN- $\beta$ , SARS-CoV-2 infection of TNF-primed cells in fact induced significant levels of IFN- $\beta$  mRNA in a dose-dependent manner (Fig 5E). In order to corroborate the central role of viral sensing through the RLRs for IFN-induction in TNF-primed cells, we stimulated RLR-deficient cells (RIG-I or MDA5 individual KO, or double KO) and checked for IFN- $\beta$  production upon infection. Depletion of RIG-I slightly reduced IFN- $\beta$  production at the mRNA (Fig 5F) and protein level (Fig EV3D), whereas IFN- $\beta$  was almost completely diminished in

MDA5<sup>KO</sup> and RIG-I/MDA5<sup>DKO</sup> cells (Figs 5F and EV3D). This effect was confirmed for the induction of the ISG RSAD2 (Fig EV3E). As expected, in contrast to IFN, TNF-pretreatment was not impacted by IFNAR deficiency, corroborating that TNF-priming is independent of type I IFN signaling (compare Fig 4). It further demonstrates that IFN- $\beta$  induction in TNF-primed cells does not require positive feedback through IFN signaling. Interestingly, IFNAR<sup>KO</sup> cells even

tended to exhibit a slight increase in sensitivity, but below statistical significance (Figs 5F and EV3D).

Overall, these data suggest that, similar to type I IFN, TNF can prime the antiviral sensing machinery of epithelial cells sufficiently to restore IFN-induction upon SARS-CoV-2 infection. This sensitization is largely mediated by MDA5, likely through its strong induction by TNF signaling.

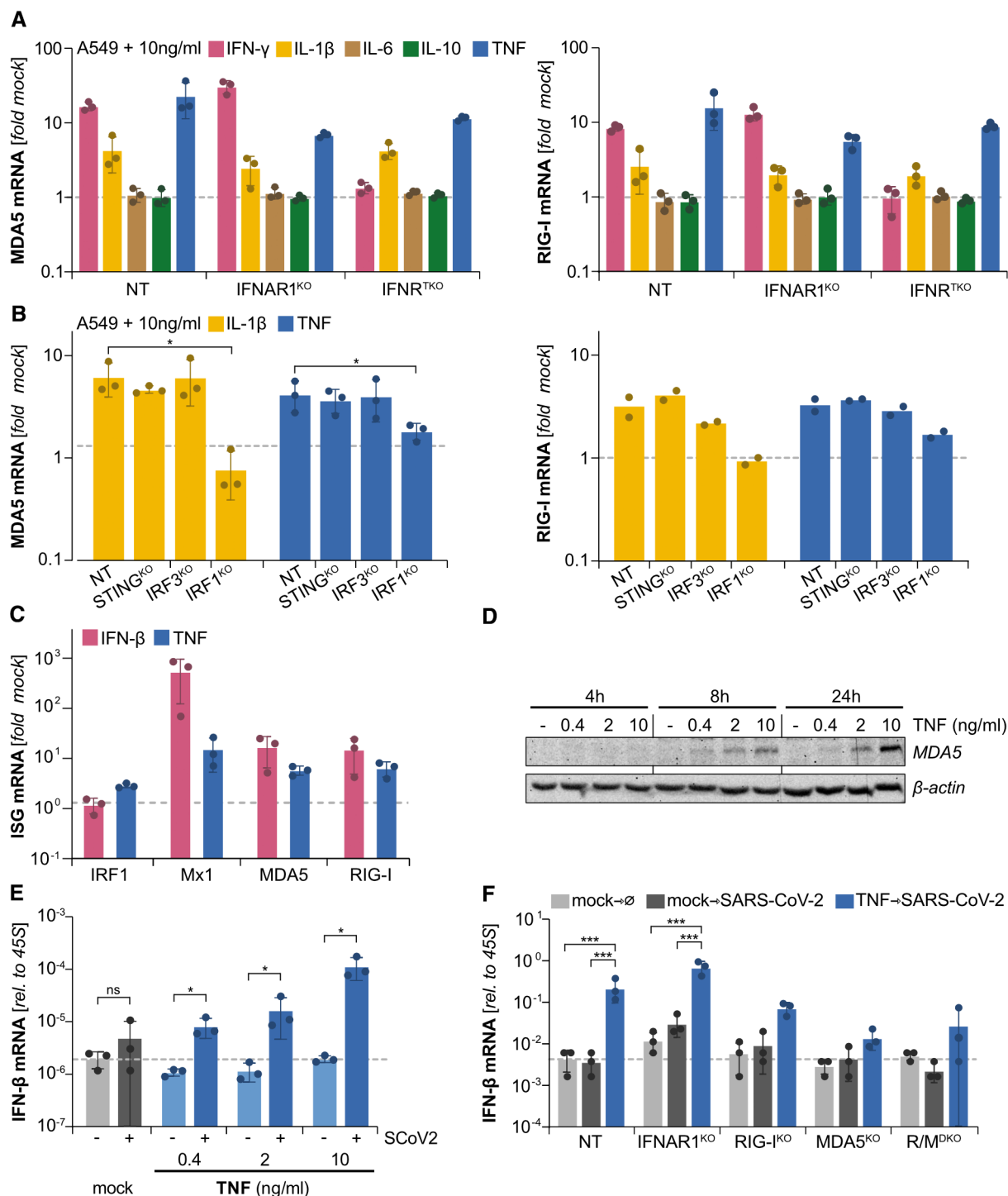


Figure 5.

**Figure 5. Epithelial cell priming by the proinflammatory cytokine TNF.**

- A A549 cells with the indicated KOs were treated with 10 ng/ml of individual recombinant human cytokines for 8 h. MDA5 (*IFIH1*) and RIG-I (*RIGI*) expression were determined by qRT-PCR. Values were normalized to GAPDH and expressed relative to mock-treated cells.
- B Indicated cell lines were treated with 10 ng/ml IL-1 $\beta$  or TNF, and MDA5 (*IFIH1*) and RIG-I (*RIGI*) expression were determined as in (A).
- C A549 cells were treated with TNF (10 ng/ml) or with IFN- $\beta$  ( $1 \times IC_{50}$ , 170 IU/ml) for 16 h. Expression of the indicated IFN-stimulated genes (ISG) was determined by qRT-PCR.
- D Western blot analysis of MDA5 in A549 cells treated with recombinant human TNF at the indicated concentrations (or mock-treated) for 4, 8, or 24 h. The blot is representative of two biological replicates.
- E A549<sup>ACE2/TMPRSS2</sup> cells were mock-treated or primed with TNF at the indicated concentrations for 8 h followed by infection with SARS-CoV-2 (MOI 1) for 24 h. IFN- $\beta$  (*IFNB1*) gene expression was determined by qRT-PCR.
- F A549<sup>ACE2/TMPRSS2</sup> wild-type (NT) cells or with the indicated KO (R/M<sup>DKO</sup>: RIG-I and MDA5 double KO) were mock-treated or primed with TNF (10 ng/ml) for 8 h followed by SARS-CoV-2 infection (MOI 1). At 24 h post infection, induction of IFN- $\beta$  (*IFNB1*) expression was determined by qRT-PCR.

Data information: In (A–C, E, and F) bars represent means  $\pm$  SD,  $n = 3$  (biological replicates, individual experiments shown as dots). (B, E and F) Statistical significance was tested by an unpaired one-tailed  $t$ -test. \* $P < 0.05$ , \*\*\* $P < 0.001$ , no asterisk: not significant.

Source data are available online for this figure.

### Immune cells from children are more effective in inducing MDA5 and mounting an antiviral defense against SARS-CoV-2

So far, our experiments have shown that immune cells, via cytokine release, can tune the antiviral responsiveness of epithelial cells, largely through regulating the expression levels of viral sensors such as RIG-I and MDA5. We observed this to be particularly prominent in the airway epithelium of children, correlating with their significantly stronger induction of antiviral responses upon SARS-CoV-2 infection as compared to adults (Loske *et al*, 2022). We now wanted to understand whether the increased number of immune cells in the mucosal tissue of children (Fig 4A) alone explains the stronger priming of epithelial cells or whether immune cells of younger individuals additionally have a higher intrinsic potential to produce cytokines and stimulate RLR expression. We obtained PBMCs from five healthy adolescents (ages 14–17, median: 15.5 years) and six adults (ages 35–66, median: 46.25 years); note these individuals were not participants in our previous scRNA-Seq study (Loske *et al*, 2022). We again stimulated the PBMCs by 1-h exposure to live Ye, after which we killed the bacteria using gentamicin (Fig 6A). Twenty-four hours later, supernatants of PBMCs were transferred to A549 cells and MDA5 and RIG-I mRNA levels were assessed after 8 h of incubation. While the supernatants of nonstimulated PBMCs had no impact on RLR expression, the supernatants of bacteria-exposed immune cells strongly induced both MDA5 and RIG-I mRNA (Fig 6B). Interestingly, PBMC supernatants of the younger individuals elicited significantly higher MDA5 expression in A549 cells than those of adults. RIG-I expression showed a similar but nonsignificant trend. When we assessed the IFN content of PBMC supernatants, we observed slightly increased protein levels of all measured IFNs (IFN- $\alpha 2$ , - $\beta$ , - $\gamma$ , and - $\lambda 1$ ) in the PBMCs of adolescents as compared to those of adults, albeit none reached statistical significance (Fig 6C, further cytokines see Fig EV4). These findings indeed argue in favor of an intrinsically more vigorous response of immune cells in younger individuals than cells in adults toward an identical stimulus.

Lastly, having observed this stronger response of juveniles' immune cells, we were curious whether this propensity would also lead to more vigorous responses to SARS-CoV-2 infection. It has previously been reported that co-cultivation of infected epithelial cells with plasmacytoid dendritic cells (pDC) allows sensing of infection and production of type I IFN by pDC (preprint: Venet *et al*, 2021). We aimed at reproducing this by co-culturing SARS-CoV-2-infected

A549<sup>ACE2/TMPRSS2</sup> cells with PBMCs from the same adolescent and adult donors as above. We added PBMCs to the epithelial cells 8 h after the SARS-CoV-2 infection. After 16 h of co-cultivation, we then determined the secreted cytokine profile (Fig 6D). While in the absence of PBMC, A549 cells once again failed to secrete appreciable amounts of IFNs (Fig EV5A), we measured substantial amounts of type I, II, and III IFNs as well as TNF in the co-culture setting (Figs 6E and EV5A). Also in this set-up, we found a statistically significant tendency of higher IFN and TNF levels in the co-cultures with PBMCs of adolescents as compared to adults (Fig 6E, further cytokines see Fig EV5B). Interestingly, this cytokine production by immune cells likely in turn sensitized virus sensing and IFN- $\beta$  production by the A549 cells, as co-culture of PBMCs with infected RLR-deficient (RIG-I/MDA5<sup>DKO</sup>) A549 cells yielded significantly lower IFN- $\beta$  and IFN- $\lambda 1$  levels (Fig EV5C).

Overall, our data indicate that in children and adolescents, epithelial cells of the nasal mucosa are potentially primed due to at least two distinct factors: (i) a higher density of immune cells in the mucosal tissue, and (ii) a more vigorous cytokine production by those immune cells. The latter most likely also contributes to a faster and stronger mounting of an antiviral response to SARS-CoV-2 infection. In effect, this likely forms the basis for the more efficient immunological control of the infection in children and the substantially lower risk of pediatric patients developing severe courses of COVID-19.

## Discussion

A strong and well-coordinated immune response is key for the successful clearance of any viral infection. A central role in the coordination of the many effector branches of the immune system is assumed by early and little-specific innate immune responses (Newton *et al*, 2016). Given the extreme replication kinetics not uncommon with viruses, a swift and potent induction of type I and III IFNs—the major antiviral mediators—by the infected cells themselves as well as, secondarily, local tissue-patrolling innate immune cells is key to the proper and timely triggering of a full-fledged and efficacious defense program. The swiftness of virus recognition and the onset of IFN production are even more important given that many viruses quickly express potent antagonists blunting specifically these immediate-early host defense pathways (Rai *et al*, 2021). This race-like situation is infamously exemplified by the recently

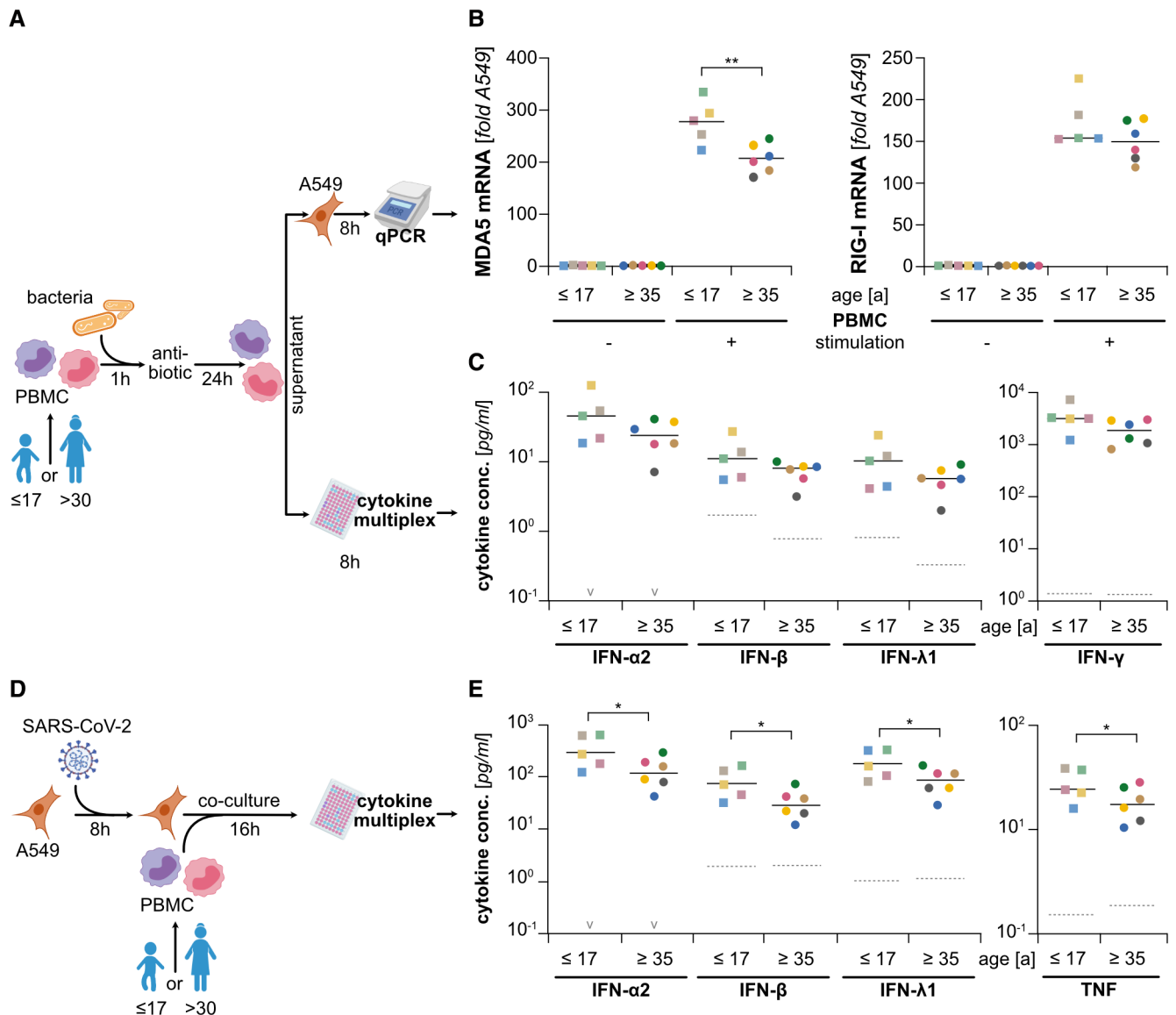


**Figure 6. Antiviral priming of epithelial cells by immune cells of juvenile versus adult donors.**

**A** PBMCs isolated from healthy juvenile (14–17 years) and adult (35–60 years) donors were mock treated or exposed to live Gram-negative bacteria (*Yersinia enterocolitica*, Ye), killed after 1 h by gentamicin treatment. After 24 h, culture supernatants were harvested and analyzed.

**B** A549 cells were incubated with the collected PBMC supernatants. After 8 h, expression of MDA5 (*IFIH1*) and RIG-I (*RIGI*) was determined by qRT-PCR. Values were normalized to GAPDH levels and expressed relative to A549 not treated with PBMC supernatant.

**C** Supernatants of mock-treated PBMCs or of PBMCs exposed to Ye were analyzed for their IFN content by electrochemiluminescent multiplex assay.

**D** A549 cells were infected with SARS-CoV-2 (MOI 0.1) for 8 h before adding PBMCs to the culture. After 16 h of co-culturing, supernatants were harvested and subjected to cytokine multiplex measurement.

**E** Levels of secreted cytokines were determined (see Fig EV5B for further cytokines).

Data information: (B, C and E) Values for each donor are shown individually ( $n = 5$  juvenile,  $n = 6$  adult donors); color identifies the donor across all measurements. Median shown as a solid black line; median of (B and C) mock stimulated samples or (E) co-culture of uninfected A549 with PBMCs shown as a dashed gray line (individual data points omitted); “v” signifies median below 10<sup>-1</sup> pg/ml. Statistical significance between juvenile and adult samples was tested by an unpaired one-tailed t-test.

\* $P < 0.05$ , \*\* $P < 0.01$ , no asterisk: not significant.

Source data are available online for this figure.

emerged SARS-CoV-2, which combines very fast replication kinetics (Cheemarla *et al*, 2021) with a versatile array of immune antagonists that effectively interfere with many steps of the cell-intrinsic antiviral system (reviewed in Lee *et al*, 2022). As a consequence,

SARS-CoV-2 infection fails to induce significant amounts of type I and III IFNs in immune-competent A549 lung epithelial cells (Blanco-Melo *et al*, 2020; Neufeldt *et al*, 2022), as we also confirm in the present study as well as in further cell culture models.

Nonetheless, some reports describe notable production of IFNs in certain cells, including lung and intestinal epithelial cells (Desai *et al*, 2020; Katsura *et al*, 2020; Stanifer *et al*, 2020). We argue that this apparent contradiction is a direct consequence of the race-like virus-host interplay early in infection, which is exceptionally dichotomized by SARS-CoV-2: either the cell senses and responds to the virus fast enough, or the virus shuts off the respective pathways virtually completely. Indeed, we here demonstrate that SARS-CoV-2 nonresponsive A549 cells can be rendered fully responsive by pretreating them with low-moderate doses of IFN or TNF, underscoring that subtle differences in the state of the host cell can be the basis of an all-or-nothing outcome in terms of IFN production.

The efficient suppression of IFN induction by SARS-CoV-2 appears to be a major determinant for viral replication and spread and, hence, for disease development. Even though viral antagonists also target IFN downstream signaling (Lee *et al*, 2022), overall the virus remains very sensitive to IFN (Felgenhauer *et al*, 2020; preprint: Lokugamage *et al*, 2020; Vanderheiden *et al*, 2020). In fact, clinical genetics studies clearly established a malfunctioning type I IFN response as a critical determinant predisposing individuals to severe and life-threatening COVID-19 (Bastard *et al*, 2020; Zhang *et al*, 2020), but with incomplete penetrance, particularly in adolescents and young adults (Meisel *et al*, 2021). While high IFN levels in the lung and serum at later stages of the disease are associated with severity (Chen *et al*, 2020; Lee *et al*, 2020; Lucas *et al*, 2020), early and local IFN production right at the primary infection site in the upper respiratory tract has been appreciated as a major determinant for successful control of infection and mild courses of disease (Park & Iwasaki, 2020; Cheemarla *et al*, 2021; Lopez *et al*, 2021; Sposito *et al*, 2021; Wong & Perlman, 2022). By single cell analyses of cells isolated from nasal swabs, we and others could show that the high resilience of children toward severe COVID-19 is associated with an increased expression of virus sensors, in particular MDA5, in airway epithelial cells already prior to infection and, consequently, with a significantly faster and stronger IFN response upon SARS-CoV-2 infection as compared to adult patients (Loske *et al*, 2022; Yoshida *et al*, 2022).

Here, we investigated the molecular basis of efficient detection of SARS-CoV-2 infection and the mounting of a proper IFN response. For this purpose, we have set up a simplified *in vitro* model based on the lung epithelial cell line A549 and validated our findings with scRNA-Seq data from nasal swab samples. A549 cells are well-known to have a functional and potent antiviral system (Wüst *et al*, 2021; Burkart *et al*, 2023), but are little responsive to SARS-CoV-2 infection, similar to what we have previously observed for airway epithelial cells of adult donors (Loske *et al*, 2022). In that study, we found the primed state of epithelial cells in children to be somewhat reminiscent of an IFN signature that included the increased expression of the RLRs. We now mimic this state *in vitro* by pretreatment of A549 cells with a rather low dose of IFN- $\beta$ . This led to the increased expression of a variety of pattern recognition receptors, allowing us to study their respective impact on functional SARS-CoV-2 recognition. It has previously been shown that MDA5 is the major receptor sensing SARS-CoV-2 in epithelial cells (Rebendenne *et al*, 2021; Sampaio *et al*, 2021; Thorne *et al*, 2021; Yin *et al*, 2021). Employing an array of CRISPR/Cas9-based functional KOs, we confirmed MDA5 as the single most important sensor in this system. Notably, there was no impact of TLR/TRIF/MyD88

or cGAS/STING pathways whatsoever in our system. However, we identified a significant contribution by RIG-I: only simultaneous depletion of both receptors, MDA5 and RIG-I, completely abrogated IFN- $\beta$  production upon SARS-CoV-2 infection. Correspondingly, moderately elevated expression of RIG-I only—in the complete absence of MDA5—sufficed to sense infection and trigger the IFN- $\beta$  response. The role of RIG-I in sensing the virus has not been widely appreciated before but was shown in one previous study (Thorne *et al*, 2022). Moreover, RIG-I has been implicated with IFN- and signaling-independent inhibition of SARS-CoV-2 replication by direct binding to the 3'-UTR of the viral genome (Yamada *et al*, 2021). In fact, in RIG-I<sup>KO</sup> cells, we even observed a slight increase in IRF3 phosphorylation and ensuing IFN- $\beta$ , which might be related to somewhat stronger viral replication (not confirmed in qRT-PCR) or increased accessibility to MDA5 in the absence of RIG-I binding.

The observed IFN-like signature in the epithelium of children as well as our IFN- $\beta$  priming approach are both associated with the induction of countless genes. However, our KO studies in A549 cells confirmed the crucial role of the RLRs for the detection of SARS-CoV-2. Furthermore, our complementary approach of expressing only either MDA5 or RIG-I on a double-KO background to levels slightly above the endogenous situation was sufficient to render cells responsive to SARS-CoV-2 infection, similar to IFN pretreatment. This supports the notion that elevated expression, specifically of RLRs, would be causal for stronger IFN production in the upper airways of children as compared to adults. It is further supported by the fact that RLR expression, in particular MDA5, is highest in infants and gradually decreases over childhood and adolescence, mirroring the increasing risk for severe disease with age (O'Driscoll *et al*, 2021). So far, it is unclear whether a further decrease in RLR expression may also be responsible for the exponentially increasing risk of severe COVID-19 in the elderly. A previous study showing reduced vigor of RIG-I signaling in monocytes of aged individuals as one aspect of immunosenescence may support this idea (Molony *et al*, 2017).

This age-dependence of the antiviral responsiveness of epithelial cells may be due to a developmental program. In fact, it has been shown that a subset of ISGs is highly expressed in the stem cell compartment and is lost during differentiation (Wu *et al*, 2018). However, this stem cell program appears to be tuned for direct antiviral effectors at the expense of the inducible IFN response, and indeed, neither RIG-I nor MDA5 are expressed at significant levels in stem cells (Wu *et al*, 2018). Alternatively, the elevated expression in the airway epithelia of infants and school-age children may be mediated by immune-epithelial cell interactions (Larsen *et al*, 2020; Hewitt & Lloyd, 2021). Interestingly, we find substantially higher proportions of immune cells in the mucosa of healthy, that is, noninfected, children as compared to adult donors (see also Loske *et al*, 2022) and we also find stronger immune-epithelial cell interactivity. We hypothesize immune cells, particularly upon frequent microbial encounter in a nonsterile environment such as the upper respiratory tract, give rise to a cytokine milieu capable of priming the antiviral sensing machinery of epithelial cells. This hypothesis was confirmed *in vitro*, where we found bacteria-exposed immune cells to potently stimulate RLR expression in epithelial A549 cells through cytokines such as IFN- $\alpha$ , IFN- $\gamma$ , TNF, and to some lesser extent, IL-1 $\beta$ . Indeed, also *in vivo*, we found IFN- $\gamma$  and TNF to be significantly higher expressed in the mucosal immune cells of healthy children than in



those of adults. Interestingly, we did not find significant expression of type I or III IFN in our scRNA-Seq data. This may be due to technical reasons, but in the organism, those IFNs are also stringently restricted to the acute phase of an infection in order to prevent harmful side effects (Crow & Stetson, 2022). Importantly, despite RIG-I and MDA5 being classical ISGs, type I IFNs were not decisive in epithelial RLR upregulation by immune cells, and even in fully IFN-blind (type I, II, and III) A549 IFN<sup>TKO</sup> cells, the RLRs were still significantly induced. This is in line with other studies in which MDA5 (Matikainen *et al*, 2006; Yarilina *et al*, 2008; Venkatesh *et al*, 2013) and RIG-I (Matikainen *et al*, 2006; Yarilina *et al*, 2008; Venkatesh *et al*, 2013) could be induced in an IFN-independent manner, for example, by TNF, leading to an enhanced response toward influenza virus (Matikainen *et al*, 2006; Yarilina *et al*, 2008; Venkatesh *et al*, 2013). Although recently both IL-1 $\beta$  and TNF were shown to lead to mitochondrial DNA release and signaling through the cGAS/STING/IRF3 pathway to induce IFNs and ISGs (Aarreberg *et al*, 2019), in KO experiments we could show that in our system RLR upregulation was completely independent of STING and IRF3, but instead almost entirely dependent on IRF1. While this was surprising at first, it is in line with reports ascribing a central role to IRF1 in regulating constitutive expression of antiviral genes, such as TLR2, TLR3, and OAS2 (Panda *et al*, 2019), and contributing to TNF- and IL-1 $\beta$ -mediated ISG expression in monocytes and epithelial cells (Yarilina *et al*, 2008; Aarreberg *et al*, 2019). Interestingly, IRF1 is also a major transcription factor downstream of IFN- $\gamma$ , making it a central regulator for the antiviral priming of airway epithelial cells. Taken together, this suggests immune cells in the respiratory mucosa tune the antiviral system of epithelial cells by creating a weak but constitutive inflammatory cytokine milieu. It remains to be elucidated whether an increased frequency of microbial encounters by children, for example, during play or generally less hygienic behavior, contributes to immune cell activation. Importantly, though, even upon experimental stimulation with equal amounts of bacteria, we observed a stronger potential of PBMCs of young donors to induce MDA5 and RIG-I expression in A549 cells as compared to adult PBMC, presumably due to a slight tendency for increased cytokine production. This once again highlights the higher reactivity of the (innate) immune system of younger individuals. The opposite effect has been described as immunosenescence, referring to less potent immune responses in the elderly (Shaw *et al*, 2013), and might very well be a major contributor to the drastic increase in morbidity and mortality of COVID-19 in the aged population. Indeed, at the time of writing this manuscript, a very elegant study reported on the molecular underpinnings of exacerbated disease in old mice (Beer *et al*, 2022). The authors identified a lack of IFN- $\gamma$  in aged mice as the driving factor behind excessive viral replication and a lack of immunological control of infection. Pretreatment of mice with exogenous IFN- $\gamma$  almost completely reverted the aged phenotype. This appears to be a perfect mirror image of our above findings of IFN- $\gamma$  (and TNF) being constitutively expressed at higher levels in the airways of young individuals, leading to antiviral priming of epithelial cells and a more potent overall immune response to SARS-CoV-2 infection.

Interestingly, while *in vitro* A549 cells did not produce notable amounts of IFNs and other cytokines in response to SARS-CoV-2 inoculation, co-cultivation of infected A549 together with PBMCs gave rise to high levels of type I, II, and III IFN, as well as increased

amounts of TNF and IL-6. This is likely caused by direct cell–cell contact of pDCs and possibly other innate immune cells with infected A549, enabling sensing of and responding to infection by the immune cells, as reported recently (preprint: Venet *et al*, 2021). In turn, this will sensitize virus sensing by the epithelial cells, as we have shown above, leading to further increased IFN production. In fact, we found the majority of IFN- $\beta$  and - $\lambda$  to be dependent on RLR sensing in epithelial cells, highlighting the complex interplay of immune and epithelial cells in the establishment of a full-fledged antiviral response. Of note, also in this setting, we found a significant tendency toward stronger cytokine production when PBMCs were from juveniles as compared to adult donors. It will be interesting to further dissect the contribution of epithelial versus immune cells to the overall cytokine production in this setting in a future study. The importance and complexity of epithelial–immune cell interactions during viral infection have only begun to be appreciated in recent years (Hewitt & Lloyd, 2021; Barnett *et al*, 2023). For example, upon SARS-CoV-2 infection, isolated epithelial cells were found not to release IL-1 $\beta$ ; however, the presence of myeloid cells primed the inflammasome system of epithelial cells, resulting in robust production and secretion of the pro-inflammatory cytokines IL-1 $\beta$  and IL-6 upon infection (Barnett *et al*, 2023).

Our study has limitations, and the proposed model clearly needs to be further tested in more authentic setups, ideally *in vivo*, in the future. In particular, our *in vitro* model is based on the lung adenocarcinoma-derived cell line A549, which might differ in various aspects from primary airway epithelial cells. Nonetheless, specifically, the cell-intrinsic antiviral response is remarkably functional in A549 cells, and they are widely accepted as a model system for this aspect. Furthermore, crude PBMCs may be a poor surrogate for tissue resident or transiently patrolling immune cells found in the healthy mucosa. We tried to alleviate these limitations by cross-checking and validating our observations in scRNA-Seq data from nasal airway swabs. While our *in vitro* findings are compatible with accumulating human data from scRNA-Seq studies (Loske *et al*, 2022; Yoshida *et al*, 2022), those *in vivo* data are only cross-sectional snapshots. Further, longitudinal experiments, for example, in animal models such as the Syrian hamster (Francis *et al*, 2021; Nouailles *et al*, 2021) or in mice (Beer *et al*, 2022), will be helpful in better understanding the complex interplay of immune and epithelial cells before and during infection.

Taken together, on the background of previous studies, our findings suggest a model of the interplay of immune cells and epithelial cells in the context of SARS-CoV-2, and probably many other virus infections. Common pro-inflammatory cytokines such as TNF or IFN- $\gamma$  are likely constitutively present at low levels in the nonsterile environment of the airway mucosa and critically tune the expression of virus-sensing pathways in epithelial cells. In younger individuals up to adolescence, both an increased number of mucosal immune cells and their higher intrinsic propensity to produce such cytokines lead to an increased expression of MDA5 and RIG-I in epithelial cells as compared to adults. Under these conditions, SARS-CoV-2 infection is recognized more readily and leads to stronger induction of epithelial type I and III IFN and a more robust epithelial cell-intrinsic antiviral defense. The high number of immune cells and their elevated sensitivity in younger individuals in turn lead to a more ready detection of infected epithelial cells and consequently a stronger ensuing immune activation, amplifying the epithelial response and

leading to a potent antiviral state of the tissue. This very likely affects the response to many, if not all, respiratory viruses. Seemingly at odds with our model, infections such as respiratory syncytial virus (RSV) or influenza virus are well-known to cause much higher morbidity among (young) children than in adults. However, it needs to be considered that those are widely circulating pathogens to which potent adaptive immune responses develop rapidly within the first few years of life (Bodewes *et al*, 2011; Andeweg *et al*, 2021), providing powerful protection against severe disease throughout most of adulthood. For the pandemic SARS-CoV-2, in contrast, individuals of all age classes were initially immuno-naïve. Interestingly, in the absence of adaptive immune responses, also RSV and influenza virus infections very likely cause more severe disease in adults as compared to children, as described for immunocompromised patients (Whitley & Monto, 2006; Chatzis *et al*, 2018) or in viral pandemics such as the 1918 “Spanish Flu,” during which large parts of the population initially were immuno-naïve (Ahmed *et al*, 2007). While this general age trend is consistent with our proposed model, the clinically observed higher morbidity of RSV (and influenza) as compared to COVID-19, particularly in neonates and infants, likely owes this to a complex combination of virological, anatomical, and immunological reasons.

In conclusion, our study sheds light on the vital contribution of immune cells to tissue homeostasis, in particular with regard to fine-tuning tissue sensitivity to virus infection. While this is likely of very broad and general relevance, we found it to be a hallmark difference between the airway mucosal innate immune response to SARS-CoV-2 infection in children and that in adults. A slight constitutive inflammatory milieu, mediated by immune cell-derived cytokines such as IFN- $\gamma$  and TNF, leads to the IRF1-dependent upregulation of the crucial virus sensors RIG-I and MDA5, and thereby to a significantly increased overall sensitivity of the epithelial cell-intrinsic antiviral system. This enables the airway epithelium to more rapidly mount an efficacious and properly coordinated immune response, favoring successful containment of virus infection. Our results suggest it may be worthwhile exploring prophylactic strategies for SARS-CoV-2 and other respiratory infections aiming at mimicking the mucosal tissue homeostasis of school-age children, for example, through inhalation of low-dose cytokine formulations (Meng *et al*, 2021).

## Materials and Methods

### Cell lines

A549 (RRID: CVCL\_LI35), Calu-3 (RRID: CVCL\_0609), and HEK-293T (RRID: CVCL\_0063) cells were cultured in Dulbecco’s modified Eagle medium (DMEM high glucose, Life Technologies) supplemented with 10% (v/v) heat-inactivated fetal bovine serum (FBS) (Thermo Fisher Scientific), 100  $\mu$ g/ml penicillin, 100  $\mu$ g/ml streptomycin (Life Technologies), and 1% nonessential amino acids (Thermo Fischer Scientific), and maintained in a humidified atmosphere containing 5% CO<sub>2</sub> at 37°C. All cells were negative for mycoplasma (Mycoplasma check, Eurofins Genomics).

A549-derived knockout cell lines for MyD88 (Krischuns *et al*, 2018), MAVS (Krischuns *et al*, 2018), RIG-I (Willemsen *et al*, 2017), MDA5 (Plociennikowska *et al*, 2021), RIG-I/MDA5 (referred to as RIG-I/MDA5<sup>DKO</sup>) (Plociennikowska *et al*, 2021), IRF3

(Urban *et al*, 2020), IRF1 (Wüst *et al*, 2021), IFNAR1 (Wüst *et al*, 2021), IFNAR1/IFNLR/IFNGR1 (referred to as IFNR<sup>TKO</sup>) (Wüst *et al*, 2021), and nontargeting CRISPR control cells (NT) (Wüst *et al*, 2021) were generated by CRISPR/Cas9 technology as described before. A549 knockout cell lines for TRIF and STING were generated using the lentiCRISPR system (Sanjana *et al*, 2014; Wüst *et al*, 2021) with the following gRNA sequences: TRIF: 5'-GTGAGGCCAGG ATCTCTCTAG-3', STING: 5'-TGTGCGCAGCTCCTCAGCC-3' were validated as shown in Fig EV1F.

A549 stably expressing RIG-I or MDA5 in RIG-I/MDA5<sup>DKO</sup> cells were produced by lentiviral transduction using a pWPI-based vector, with transgene expression of codon-optimized RIG-I and MDA5 under the control of the murine ROSA26 promoter, which has a weak promoter activity in human cells. Empty vector controls were generated accordingly.

### Generation of PBMC

Peripheral blood mononuclear cells (PBMC) for bacterial stimulation were isolated from the Buffy coats of healthy volunteers, obtained through ZKT Tübingen GmbH. Buffy coats were diluted 1:7 with Dulbecco’s PBS (Life Technologies). PBMCs were obtained by density gradient centrifugation at 1,000 g for 20 min at room temperature with a 35-ml cell suspension stacked on 15 ml of BioColl separation solution (Biochrom). The interphase containing PBMCs was abstracted and washed twice with PBS. PBMCs were frozen in aliquots of  $2 \times 10^7$  cells in RPMI1640 containing 20% FBS and 10% DMSO at  $-150^\circ\text{C}$  until further use. The study was approved by the local ethics committee (240/2018BO2) and complies with the declaration of Helsinki and the good clinical practice guidelines on the approximation of the laws, regulations, and administrative provisions of the member states relating to the implementation of good clinical practice in the conduct of clinical trials on medicinal products for human use.

Peripheral blood mononuclear cells of donors of specific ages were obtained from participants of the COVID-19 household study in Baden-Württemberg, Germany. This study was initiated by the University Children’s Hospitals in Freiburg, Heidelberg, Tübingen, and Ulm and approved by the respective independent ethics committees of each center. Blood samples for this substudy were collected at study site Ulm in July 2020. Epidemiological and serological data describing the larger cohort have been published previously (Stich *et al*, 2021; Haddad *et al*, 2022; Renk *et al*, 2022). The study is registered at the German Clinical Trials Register (DRKS), study ID 00021521, conducted according to the Declaration of Helsinki. For the present study, only donors were included that had no history of COVID-19 as well as had tested negative in three serological assays (EuroImmun-Anti-SARS-CoV-2 ELISA IgG/S1/, Siemens Healthineers SARS-CoV-2 IgG/RBD/, and Roche Elecsys Ig /Nucleocapsid Pan Ig/). PBMCs were selected from heparinized full blood by a standard density gradient (Pancoll Separating Solution, PAN-Biotech), and cryopreserved in medium containing 75% FBS, 15% RPMI (PAN-Biotech), and 10% DMSO (Serva) at  $-196^\circ\text{C}$  in liquid nitrogen until further analysis.

### Cytokine stimulation

A549 IFNAR1<sup>KO</sup>, IFNR<sup>TKO</sup>, and the corresponding NT control cells were seeded at a density of  $1.5 \times 10^5$  cells per well in 500  $\mu$ l of

supplemented DMEM. The next day, cells were stimulated with 10 ng/ml of TNF (ab259410, Abcam), IL-6 (7270-IL, R&D Systems), IL-1 $\beta$  (ALX-502-001, Enzo Life Sciences), IL-10 (ab259402, Abcam), and IFN- $\gamma$  (285-IF-100/CF, R&D Systems). After 8 h, cells were washed with PBS and lysed by adding 300  $\mu$ l of Monarch RNA Lysis Buffer and stored frozen  $-80^{\circ}\text{C}$  until further analysis.

## Infection

For infection with SARS-CoV-2, A549 cells were seeded in a 24-well plate at a density of  $4 \times 10^4$  cells. The next day, cells were transiently transduced with lentiviral vectors coding for ACE2 and TMPRSS2. In order to ensure homogeneous high-efficiency transduction, A549 cells were incubated with lentiviral supernatants diluted 1:20 (v/v) in culture medium containing 10  $\mu$ g/ml polybrene (Merck Millipore) and centrifuged at  $805 \times g$  at  $20^{\circ}\text{C}$  for 30 min. At 24 h posttransduction, cells were either mock-stimulated or stimulated with 170 U/ml IFN- $\beta$  or 10 ng/ml TNF for 16 and 8 h, respectively. After stimulus, cells were washed once with PBS and incubated with 200  $\mu$ l/well of DMEM containing SARS-CoV-2 at an MOI of 0.1 (IFN- $\beta$ ) and 1 (TNF). One hour after inoculation, cells were washed once with PBS and fed with 500  $\mu$ l/well of DMEM supplement with 2% FCS. Twenty-four hours after inoculation, cells were washed once with PBS and lysed for qPCR and western blot analyses. The experiments involving viral infections were conducted within a Biosafety Level 3 (BSL-3) facility at the German Cancer Research Center (DKFZ).

## RNA isolation and RT-qPCR

Total RNA was isolated from cells using the Monarch Total RNA Miniprep Kit (New England Biolabs), employing on-column digestion of residual DNA by DNaseI treatment, according to the manufacturer's instructions. Isolated RNA was reverse transcribed using the High Capacity cDNA Reverse Transcription Kit (Thermo Fisher Scientific) with random hexamer primers according to the manufacturer's specifications. Transcript levels were assessed by real-time PCR using the iTAQ Universal SYBR Green Supermix (BioRad) on a BioRad CFX 96 Real-Time PCR Detection System. Primers for qPCR were used as the following:

SARS-CoV-2-ORF1 forward: 5'-GAGAGCCTTGTCCTGGTTT-3', SARS-CoV-2-ORF1 reverse: 5'-AGTCTCCAAAGCCACGTACG-3', IFIH1 (MDA5) forward: 5'-TCGTCAAACAGGAAACAATGA-3', IFIH1 reverse: 5'-GTTATTCTCCATGCCCCAGA-3', RIGI (RIG-I) forward: 5'-CCCTGGTTTAGGAGGAAGA-3', RIGI reverse: 5'-TCCCAACTTTCAATGGCTTC-3', IFNB1 (IFN- $\beta$ ) forward: 5'-CGCCGCATTGACCATCTA-3', IFNB1 reverse: 5'-GACATTAGCCAGGAGGTTCTC-3', GAPDH forward: 5'-CGGAGTCAACGGATTGGT-3', GAPDH reverse: 5'-TTCCTTCTCAGCCTTGAC-3', 45S rRNA forward: 5'-GAACGGTGGTGTGTCGTT-3', 45S rRNA reverse: 5'-GCGTCTCGTCTCGTCTCACT-3', RSAD2 forward: 5'-CGTGAGCATCGTGAGCAATG-3', RSAD2 reverse: 5'-CTTCTTTCCTTGCCACGG-3', IFIT1 forward: 5'-GAATAGCCAGATCTCAGAGGAGC-3', IFIT1 reverse: 5'-CCATTTGTACTCATGGTTGCTGT-3'.

Quantification of target gene expression was done using the  $\Delta\text{CT}$  method (normalization to housekeeping gene only) or  $\Delta\Delta\text{CT}$  method (normalization to housekeeping gene and to a reference cell line/condition).

## Western blotting

Mock and infected samples were lysed with 100  $\mu$ l of sample buffer (30 mM Tris [pH 6.8], 0.05% bromophenol blue, 10% glycerol, 1% SDS, and 2.5%  $\beta$ -mercaptoethanol) supplemented with 1  $\mu$ l of benzonase to cleave contaminant DNA. Denaturation was obtained by heating at  $95^{\circ}\text{C}$  for 5 min. Samples were subjected to SDS-PAGE on a 10% polyacrylamide gel for 90 min at 100 V and blotted onto a polyvinylidene (PVDF) membrane (0.2  $\mu$ m) by wet transfer for 120 min at 350 mA. Membranes were blocked with blocking buffer (5% BSA in TBS containing 0.1% Tween 20) for 1 h at room temperature, followed by overnight incubation with primary antibodies on a shaker at  $4^{\circ}\text{C}$ . After washes with TBS containing 0.1% Tween (TBS-T), membranes were incubated with horse radish peroxidase (HRP)-conjugated secondary antibody for 1 h in blocking buffer at room temperature. Membranes were rewashed  $3 \times$  with TBS-T, and proteins were visualized using the Clarity Western ECL substrate (Bio-Rad) and a high-sensitive charge-coupled device (CCD) camera (ChemoCam Imager 3.2; INTAS). Images were processed by the ImageJ/Fiji software.

The following commercially available antibodies were used: rabbit monoclonal antibodies anti-p-IRF3 (S396) (#4947S, RRID: AB\_823547), anti p-STAT1 (Y701) (#7649S, RRID: AB\_10950970), anti-STAT2 (#72604S, RRID: AB\_2799824), anti p-STAT2 (Y690) (#D3P2P, RRID: AB\_2773718) were purchased from Cell Signaling Technology. Mouse monoclonal antibodies anti-GAPDH (sc-47724, RRID: AB\_627678) and anti-IRF3 (sc-3361, RRID: AB\_627826) were from Santa Cruz Biotechnology. Mouse monoclonal anti-RIG-I (AG-20B-0009, RRID: AB\_2490189) and anti-STAT1 (610115, RRID: AB\_397521) were obtained from Adipogen and BD Biosciences, respectively. Rabbit polyclonal anti-MDA5 (ALX-210-935-C100, RRID: AB\_2051837) was purchased from Enzo Life Sciences and mouse monoclonal anti- $\beta$ -actin (A5441, RRID: AB\_476744), along with anti-mouse and anti-rabbit antibodies coupled with HRP (A4416, RRID: AB\_258167; A6154, RRID: AB\_258284) were obtained from Sigma-Aldrich.

## Stimulation and infection of PBMC

Isolated PBMCs were thawed in a  $37^{\circ}\text{C}$  water bath, mixed with 9 ml of culture medium supplemented with 50 KU DNase I (Millipore), and centrifuged at  $350 \times g$  for 10 min. The supernatant was then aspirated and cells resuspended in 5 ml of culture medium containing 200 KU DNaseI, kept at  $4^{\circ}\text{C}$  for 20 min, and viable cells quantified by trypan blue. PBMCs were seeded at  $1 \times 10^6$ /ml into 24-well tissue plates. For stimulation with *Yersinia enterocolitica* (WA-314, serotype O:8), the bacterial stock was pelleted, washed once with PBS, resuspended in culture medium, and mixed with PMBC at a ratio of one bacterium per cell for 1 h. Bacterial growth was inhibited by supplementing media with 20  $\mu$ g/ml gentamicin (Biochrom). At 24 h post-treatment, cell suspensions were collected, centrifuged at  $1,000 \times g$  for 5 min, and the resultant supernatants were frozen at  $-80^{\circ}\text{C}$  until further analysis.

## Co-culture of A549 and PBMC

For co-culture experiments, A549<sup>ACE2/TMPRSS2</sup> were mock infected or infected with SARS-CoV-2 for 8 h, followed by incubation with

$1 \times 10^6$  isolated PBMCs in 1 ml of culture medium in a 24-well plate. Cell suspensions were collected after 16 h co-culture, centrifuged at  $1,000 \times g$  for 5 min and supernatants were harvested and treated with 0.1% beta-propiolactone at room temperature for 1 h and at 37°C for 2 h. Samples were stored at  $-80^\circ\text{C}$  until further analysis.

### dsRNA stimulation via electroporation

To synchronously stimulate the RIG-I pathway in A549 cells, electro-transfection was used as described in (Burkart *et al*, 2023). Briefly,  $4 \times 10^6$  mock-treated or IFN-treated cells were resuspended in 400  $\mu\text{l}$  of cytomix buffer (120 mM KCl, 0.15 mM  $\text{CaCl}_2$ , 10 mM  $\text{KPO}_4$ , 25 mM HEPES, 2 mM EGTA, and 2 mM  $\text{MgCl}_2$ ) and transferred to a 0.4 cm cuvette chamber containing 220 ng of *in vitro* generated 400-bp 5' ppp-dsRNA (Binder *et al*, 2011). The suspension was electroporated using the Gene Pulser Xcell modular system (150 V, 10 ms exponential decay). Electroporated cells were transferred to prewarmed DMEM and washed twice with DMEM before being distributed on 6-well plates containing  $5 \times 10^5$  cells in 1.2 ml of medium per well. At the indicated time points, cells were washed once with PBS and lysed for qPCR analysis.

### Read-out by MSD electrochemiluminescent multiplex assay

To quantify the level of released IFN, chemokine, and proinflammatory cytokines, the supernatants of mock and stimulated PBMCs were subjected to electrochemiluminescent multiplex assay using kits from Meso Scale Discovery. IFN- $\alpha 2$ , IFN- $\beta$ , IFN- $\lambda 1$  (IL-29), and IFN- $\gamma$  were measured with human U-PLEX Interferon Combo (K15094K), whereas the proinflammatory cytokines IL1- $\beta$ , IL-6, and TNF were determined using the human V-PLEX Proinflammatory Panel 1 Kit (K15049D). Production of GM-CSF, IL-2, IL-4, IL-8, IL-10, and IL12p70 were detected by a customized U-PLEX Biomarker Group 1 (K15067L). Assays were performed according to the manufacturer's instructions, read out by the MSD Quickplex SQ120 device, and data evaluated using the MSD Discovery Workbench software (version 4.0). Values below the limits of quantification (LLOQ) were denoted as not detectable (nd).

### Single cell RNA sequencing data analysis

Single cell data, including details on sample preparation, study participants (exact ages), and the molecular definition of cell types and states was reported previously (Loske *et al*, 2022) and is publicly available as a Seurat object (doi: [10.6084/m9.figshare.14938755](https://doi.org/10.6084/m9.figshare.14938755)). Briefly, nasal airway swabs of healthy and SARS-CoV-2-infected children and adults were obtained and analyzed by single-cell RNA sequencing (scRNA-Seq). For the present study, further analyses were performed exclusively based on the samples of healthy donors, comprising 18 children (4.03–16.11 years, median age 9.0 years) and 23 adults (24–77 years, median age 46.0 years). Therefore, the Seurat object was subsetted to only SARS-CoV-2 negative samples using the subset function of Seurat (<https://github.com/satijalab/seurat>). The final object had 114,296 cells (SARS-CoV-2-negative children 51,595; negative adults 62,701). For all scRNA-Seq analyses Seurat 3.2.2 was used.

Cell–cell interaction analyses of scRNA-Seq data were performed using CellChat 1.5.0 (Jin *et al*, 2021). The interaction database was

augmented with novel interaction pairs identified by Shilts *et al* (2022). Only interactions emanating from immune cells, that is, with ligands being expressed by immune cells, and targeting receptor-expressing epithelial cells were retained. Pathway-level interactions were derived using the built-in annotations of CellChat.

### Statistical analysis

Unless stated otherwise, experiments have been repeated three times on different days (i.e., biological replicates), with each repetition comprising duplicate or triplicate wells (i.e., technical replicates). Shown are mean values with error bars representing standard deviations (SD), always representing the means and SD across independent repetitions (with technical replicates averaged before). For the sake of transparency, means of each repetition are displayed as individual data points in the graphs.

Differences between two data sets were tested for statistical significance by an unpaired, one-tailed Student's *t*-test if not stated otherwise. We used one-tailed tests as all experiments study effects in a predefined direction (*induction* of gene expression/cytokine production or *inhibition* of virus replication), and the null hypothesis was formulated accordingly. Statistical analyses and data plotting were performed using GraphPad Prism (v.9).

*P*-values for violin plots showing MDA5 and RIG-I expression levels across all epithelial cells were calculated using the Seurat function FindMarkers(), applying the Wilcoxon test, and adjusted with Bonferroni correction. Age-groups were chosen such that they reflect the actual ages of participants (4–7:  $n = 5$ , 8–11:  $n = 8$ , 12–16:  $n = 5$ ); binning in the classical 0–6, 7–10, 11–18 groups did not change statistical significance.

*P*-values for violin plots showing average cytokine expression in immune cells across samples were calculated using the ks.test function of R and corrected with the Benjamini-Hochberg method (Benjamini & Hochberg, 1995).

## Data availability

No large primary datasets have been generated and deposited.

**Expanded View** for this article is available [online](#).

### Acknowledgements

The authors thank Nadine Gillich for help in generating and characterizing the MDA5<sup>KO</sup> and RIG-I/MDA5<sup>DKO</sup> cell lines, Manina Günther for excellent help and guidance handling PBMCs and Ye, and Dongsheng Yuan for help in scRNA-Seq data analysis. We are grateful to Ralf Bartschlagler for providing an outstanding research environment and critical discussions. We thank all patients and healthy volunteers who donated nasal swab samples or blood (PBMC) used in this study and Sebastian Stricker for help with the collection of nasal swabs. We further thank Maximilian Stich and Daniel Schnepf for their critical reading of the manuscript. We apologize to all colleagues whose work we did not properly cite due to space limitations and/or our lack of oversight of the extensive amount of literature on COVID-19. Figures with schematic illustrations were made with [biorender.com](https://biorender.com). This work was supported by grants from the German Research Foundation (DFG) (BI1693/2-1, BI1693/1-2 and project 272983813 TRR179/TP11 to MB; project 431232613 SFB1449/TP A01, Z01 to MAM), the fightCOVID@DKFZ intramural initiative (to

MB), the German Federal Ministry of Education and Research (BMBF) (RECAST 01IK20337 to JR and MAM; 82DZL009B1 to MAM, the Medical Informatics Initiative grant 01ZZ2001 to RE and SL) and by the Ministry of Science, Research and Arts Baden-Württemberg within the framework of the special funding line for COVID-19 research (to AJ). Special funding for the single-cell analyses within this study was obtained from the intramural BIH COVID-19 research program. SSB was supported by the Helmholtz International Graduate School at DKFZ. The funders had no role in the study design, data collection, data analysis, or the decision to publish. Open Access funding enabled and organized by Projekt DEAL.

## Author contributions

**Vladimir G Magalhães:** Conceptualization; data curation; formal analysis; validation; investigation; visualization; methodology; writing – original draft; writing – review and editing. **Sören Lukassen:** Data curation; software; formal analysis; visualization; writing – review and editing. **Maïke Drechsler:** Data curation; formal analysis; investigation. **Jennifer Loske:** Data curation; software; formal analysis; visualization; writing – review and editing. **Sandy S Burkart:** Data curation; formal analysis; investigation; visualization. **Sandra Wüst:** Validation; investigation. **Eva-Maria Jacobsen:** Resources; writing – review and editing. **Jobst Röhmel:** Resources; writing – review and editing. **Marcus A Mall:** Resources; funding acquisition; writing – review and editing. **Klaus-Michael Debatin:** Resources; funding acquisition; writing – review and editing. **Roland Eils:** Resources; formal analysis; funding acquisition; writing – review and editing. **Stella Autenrieth:** Resources; formal analysis; writing – review and editing. **Aleš Janda:** Resources; funding acquisition; writing – review and editing. **Irina Lehmann:** Resources; formal analysis; funding acquisition; writing – review and editing. **Marco Binder:** Conceptualization; formal analysis; supervision; funding acquisition; visualization; writing – original draft; project administration; writing – review and editing.

## Disclosure and competing interests statement

The authors declare that they have no conflict of interest.

## References

- Aarreberg LD, Esser-Nobis K, Driscoll C, Shuvarikov A, Roby JA, Gale M Jr (2019) Interleukin-1 $\beta$  induces mtDNA release to activate innate immune signaling via cGAS-STING. *Mol Cell* 74: 801–815
- Ahmed R, Oldstone MB, Palese P (2007) Protective immunity and susceptibility to infectious diseases: lessons from the 1918 influenza pandemic. *Nat Immunol* 8: 1188–1193
- Andeweg SP, Schepp RM, van de Kasstelee J, Mollema L, Berbers GAM, van Boven M (2021) Population-based serology reveals risk factors for RSV infection in children younger than 5 years. *Sci Rep* 11: 8953
- Asano T, Boisson B, Onodi F, Matuozzo D, Moncada-Velez M, Maglorius Renkilaraj MRL, Zhang P, Meertens L, Bolze A, Materna M et al (2021) X-linked recessive TLR7 deficiency in ~1% of men under 60 years old with life-threatening COVID-19. *Sci Immunol* 6: eabl4348
- Barnett KC, Xie Y, Asakura T, Song D, Liang K, Taft-Benz SA, Guo H, Yang S, Okuda K, Gilmore RC et al (2023) An epithelial-immune circuit amplifies inflammasome and IL-6 responses to SARS-CoV-2. *Cell Host Microbe* 31: 243–259
- Bastard P, Rosen LB, Zhang Q, Michailidis E, Hoffmann HH, Zhang Y, Dorgham K, Philippot Q, Rosain J, Béziat V et al (2020) Autoantibodies against type I IFNs in patients with life-threatening COVID-19. *Science* 370: eabd4585
- Beer J, Crotta S, Breithaupt A, Ohnemus A, Becker J, Sachs B, Kern L, Llorian M, Ebert N, Labrousse F et al (2022) Impaired immune response drives age-dependent severity of COVID-19. *J Exp Med* 219: e20220621
- Benjamini Y, Hochberg Y (1995) Controlling the false discovery rate: a practical and powerful approach to multiple testing. *J R Stat Soc B Methodol* 57: 289–300
- Binder M, Eberle F, Seitz S, Mücke N, Hüber CM, Kiani N, Kaderali L, Lohmann V, Dalpke A, Bartenschlager R (2011) Molecular mechanism of signal perception and integration by the innate immune sensor retinoic acid-inducible gene-I (RIG-I). *J Biol Chem* 286: 27278–27287
- Blanco-Melo D, Nilsson-Payant BE, Liu WC, Uhl S, Hoagland D, Moller R, Jordan TX, Oishi K, Panis M, Sachs D et al (2020) Imbalanced host response to SARS-CoV-2 drives development of COVID-19. *Cell* 181: 1036–1045
- Bodewes R, de Mutsert G, van der Klis FR, Ventresca M, Wilks S, Smith DJ, Koopmans M, Fouchier RA, Osterhaus AD, Rimmelzwaan GF (2011) Prevalence of antibodies against seasonal influenza A and B viruses in children in Netherlands. *Clin Vaccine Immunol* 18: 469–476
- Burkart SS, Schweinösch D, Frankish J, Sparr C, Wüst S, Urban C, Merlo M, Magalhães VG, Piras A, Pichlmair A et al (2023) High-resolution kinetic characterization of the RIG-I-signaling pathway and the antiviral response. *Life Sci Alliance* 6: e202302059.
- Chatzis O, Darbre S, Pasquier J, Meylan P, Manuel O, Aubert JD, Beck-Popovic M, Masouridi-Levrat S, Ansari M, Kaiser L et al (2018) Burden of severe RSV disease among immunocompromised children and adults: a 10 year retrospective study. *BMC Infect Dis* 18: 111
- Cheemarla NR, Watkins TA, Mihaylova VT, Wang B, Zhao D, Wang G, Landry ML, Foxman EF (2021) Dynamic innate immune response determines susceptibility to SARS-CoV-2 infection and early replication kinetics. *J Exp Med* 218: e20210583
- Chen N, Zhou M, Dong X, Qu J, Gong F, Han Y, Qiu Y, Wang J, Liu Y, Wei Y et al (2020) Epidemiological and clinical characteristics of 99 cases of 2019 novel coronavirus pneumonia in Wuhan, China: a descriptive study. *Lancet* 395: 507–513
- Chu H, Chan JF, Wang Y, Yuen TT, Chai Y, Hou Y, Shuai H, Yang D, Hu B, Huang X et al (2020a) Comparative replication and immune activation profiles of SARS-CoV-2 and SARS-CoV in human lungs: an *ex vivo* study with implications for the pathogenesis of COVID-19. *Clin Infect Dis* 71: 1400–1409
- Chu H, Chan JF-W, Yuen TT-T, Shuai H, Yuan S, Wang Y, Hu B, Yip CC-Y, Tsang JO-L, Huang X et al (2020b) Comparative tropism, replication kinetics, and cell damage profiling of SARS-CoV-2 and SARS-CoV with implications for clinical manifestations, transmissibility, and laboratory studies of COVID-19: an observational study. *Lancet Microbe* 1: e14–e23
- Crow YJ, Stetson DB (2022) The type I interferonopathies: 10 years on. *Nat Rev Immunol* 22: 471–483
- Desai N, Neyaz A, Szabolcs A, Shih AR, Chen JH, Thapar V, Nieman LT, Soloviyov A, Mehta A, Lieb DJ et al (2020) Temporal and spatial heterogeneity of host response to SARS-CoV-2 pulmonary infection. *Nat Commun* 11: 6319
- Felgenhauer U, Schoen A, Gad HH, Hartmann R, Schaubmar AR, Failing K, Drosten C, Weber F (2020) Inhibition of SARS-CoV-2 by type I and type III interferons. *J Biol Chem* 295: 13958–13964
- Forero A, Ozarkar S, Li H, Lee CH, Hemann EA, Nadjombati MS, Hendricks MR, So L, Green R, Roy CN et al (2019) Differential activation of the transcription factor IRF1 underlies the distinct immune responses elicited by type I and type III interferons. *Immunity* 51: 451–464



- Francis ME, Goncin U, Kroeker A, Swan C, Ralph R, Lu Y, Etzioni AL, Falzarano D, Gerdt S, Machtaler S *et al* (2021) SARS-CoV-2 infection in the Syrian hamster model causes inflammation as well as type I interferon dysregulation in both respiratory and non-respiratory tissues including the heart and kidney. *PLoS Pathog* 17: e1009705
- Haddad A, Janda A, Renk H, Stich M, Frieh P, Kaier K, Lohrmann F, Nieters A, Willems A, Huzly D *et al* (2022) Long COVID symptoms in exposed and infected children, adolescents and their parents one year after SARS-CoV-2 infection: a prospective observational cohort study. *EBioMedicine* 84: 104245
- Hayn M, Hirschenberger M, Koepke L, Nchioua R, Straub JH, Klute S, Hunszinger V, Zech F, Prelli Bozzo C, Aftab W *et al* (2021) Systematic functional analysis of SARS-CoV-2 proteins uncovers viral innate immune antagonists and remaining vulnerabilities. *Cell Rep* 35: 109126
- Hewitt RJ, Lloyd CM (2021) Regulation of immune responses by the airway epithelial cell landscape. *Nat Rev Immunol* 21: 347–362
- Jin S, Guerrero-Juarez CF, Zhang L, Chang I, Ramos R, Kuan CH, Myung P, Plikus MV, Nie Q (2021) Inference and analysis of cell-cell communication using CellChat. *Nat Commun* 12: 1088
- Jones TC, Biele G, Mühlemann B, Veith T, Schneider J, Beheim-Schwarzbach J, Bleicker T, Tesch J, Schmidt ML, Sander LE *et al* (2021) Estimating infectiousness throughout SARS-CoV-2 infection course. *Science* 373: eabi5273
- Katsura H, Sontake V, Tata A, Kobayashi Y, Edwards CE, Heaton BE, Konkimalla A, Asakura T, Mikami Y, Fritch EJ *et al* (2020) Human lung stem cell-based alveolospheres provide insights into SARS-CoV-2-mediated interferon responses and pneumocyte dysfunction. *Cell Stem Cell* 27: 890–904
- Khanmohammadi S, Rezaei N (2021) Role of Toll-like receptors in the pathogenesis of COVID-19. *J Med Virol* 93: 2735–2739
- Krischuns T, Günl F, Henschel L, Binder M, Willemsen J, Schloer S, Rescher U, Gerlt V, Zimmer G, Nordhoff C *et al* (2018) Phosphorylation of TRIM28 enhances the expression of IFN- $\beta$  and proinflammatory cytokines during HPAIV infection of human lung epithelial cells. *Front Immunol* 9: 2229
- Lamers MM, Haagmans BL (2022) SARS-CoV-2 pathogenesis. *Nat Rev Microbiol* 20: 270–284
- Larsen SB, Cowley CJ, Fuchs E (2020) Epithelial cells: liaisons of immunity. *Curr Opin Immunol* 62: 45–53
- Lee SJ, Jang BC, Lee SW, Yang YI, Suh SI, Park YM, Oh S, Shin JG, Yao S, Chen L *et al* (2006) Interferon regulatory factor-1 is prerequisite to the constitutive expression and IFN-gamma-induced upregulation of B7-H1 (CD274). *FEBS Lett* 580: 755–762
- Lee JS, Park S, Jeong HW, Ahn JY, Choi SJ, Lee H, Choi B, Nam SK, Sa M, Kwon JS *et al* (2020) Immunophenotyping of COVID-19 and influenza highlights the role of type I interferons in development of severe COVID-19. *Sci Immunol* 5: eabd1554
- Lee JH, Koepke L, Kirchhoff F, Sparrer KMJ (2022) Interferon antagonists encoded by SARS-CoV-2 at a glance. *Med Microbiol Immunol* 212: 125–131
- Lokugamage KG, Hage A, de Vries M, Valero-Jimenez AM, Schindewolf C, Dittmann M, Rajsbaum R, Menachery VD (2020) Type I interferon susceptibility distinguishes SARS-CoV-2 from SARS-CoV. *bioRxiv* <https://doi.org/10.1101/2020.03.07.982264> [PREPRINT]
- Lopez J, Mommert M, Mouton W, Pizzorno A, Brengel-Pesce K, Mezidi M, Villard M, Lina B, Richard JC, Fassier JB *et al* (2021) Early nasal type I IFN immunity against SARS-CoV-2 is compromised in patients with autoantibodies against type I IFNs. *J Exp Med* 218: e20211211
- Loske J, Rohmel J, Lukassen S, Stricker S, Magalhães VG, Liebig J, Chua RL, Thurmman L, Messingschlager M, Seegebarth A *et al* (2022) Pre-activated antiviral innate immunity in the upper airways controls early SARS-CoV-2 infection in children. *Nat Biotechnol* 40: 319–324
- Lucas C, Wong P, Klein J, Castro TBR, Silva J, Sundaram M, Ellingson MK, Mao T, Oh JE, Israelow B *et al* (2020) Longitudinal analyses reveal immunological misfiring in severe COVID-19. *Nature* 584: 463–469
- Matikainen S, Siren J, Tissari J, Veckman V, Pirhonen J, Severa M, Sun Q, Lin R, Meri S, Uze G *et al* (2006) Tumor necrosis factor alpha enhances influenza A virus-induced expression of antiviral cytokines by activating RIG-I gene expression. *J Virol* 80: 3515–3522
- Meisel C, Akbil B, Meyer T, Lankes E, Corman VM, Staudacher O, Unterwaller N, Kolsch U, Drosten C, Mall MA *et al* (2021) Mild COVID-19 despite autoantibodies against type I IFNs in autoimmune polyendocrine syndrome type 1. *J Clin Invest* 131: e150867
- Meng Z, Wang T, Chen L, Chen X, Li L, Qin X, Li H, Luo J (2021) The effect of recombinant human interferon alpha nasal drops to prevent COVID-19 pneumonia for medical staff in an epidemic area. *Curr Top Med Chem* 21: 920–927
- Molony RD, Nguyen JT, Kong Y, Montgomery RR, Shaw AC, Iwasaki A (2017) Aging impairs both primary and secondary RIG-I signaling for interferon induction in human monocytes. *Sci Signal* 10: eaan2392
- Murtas D, Maric D, De Giorgi V, Reinboth J, Worschech A, Fetsch P, Filie A, Ascierto ML, Bedognetti D, Liu Q *et al* (2013) IRF-1 responsiveness to IFN- $\gamma$  predicts different cancer immune phenotypes. *Br J Cancer* 109: 76–82
- Neeland MR, Bannister S, Clifford V, Nguyen J, Dohle K, Overmars I, Toh ZQ, Anderson J, Donato CM, Sarkar S *et al* (2021) Children and adults in a household cohort study have robust longitudinal immune responses following SARS-CoV-2 infection or exposure. *Front Immunol* 12: 741639
- Neufeldt CJ, Cerikan B, Cortese M, Frankish J, Lee JY, Plociennikowska A, Heigwer F, Prasad V, Joecks S, Burkart SS *et al* (2022) SARS-CoV-2 infection induces a pro-inflammatory cytokine response through cGAS-STING and NF-kappaB. *Commun Biol* 5: 45
- Newton AH, Cardani A, Braciale TJ (2016) The host immune response in respiratory virus infection: balancing virus clearance and immunopathology. *Semin Immunopathol* 38: 471–482
- Ng WH, Tiph T, Makoah NA, Vermeulen JC, Goedhals D, Sempa JB, Burt FJ, Taylor A, Mahalingam S (2021) Comorbidities in SARS-CoV-2 patients: a systematic review and meta-analysis. *MBio* 12: e03647-20
- Nilsson-Payant BE, Uhl S, Grimont A, Doane AS, Cohen P, Patel RS, Higgins CA, Acklin JA, Bram Y, Chandar V *et al* (2021) The NF-kappaB transcriptional footprint is essential for SARS-CoV-2 replication. *J Virol* 95: e0125721
- Nouailles G, Wyler E, Pennitz P, Postmus D, Vladimirova D, Kazmierski J, Pott F, Dietert K, Muelleder M, Farztdinov V *et al* (2021) Temporal omics analysis in Syrian hamsters unravel cellular effector responses to moderate COVID-19. *Nat Commun* 12: 4869
- O'Driscoll M, Ribeiro Dos Santos G, Wang L, Cummings DAT, Azman AS, Paireau J, Fontanet A, Cauchemez S, Salje H (2021) Age-specific mortality and immunity patterns of SARS-CoV-2. *Nature* 590: 140–145
- Panda D, Gjinaj E, Bachu M, Squire E, Novatt H, Ozato K, Rabin RL (2019) IRF1 maintains optimal constitutive expression of antiviral genes and regulates the early antiviral response. *Front Immunol* 10: 1019
- Park A, Iwasaki A (2020) Type I and type III interferons - induction, signaling, evasion, and application to combat COVID-19. *Cell Host Microbe* 27: 870–878
- Plociennikowska A, Frankish J, Moraes T, Del Prete D, Kahnt F, Acuna C, Slezak M, Binder M, Bartenschlager R (2021) TLR3 activation by Zika virus stimulates inflammatory cytokine production which dampens the antiviral response induced by RIG-I-like receptors. *J Virol* 95: e01050-20
- Rai KR, Shrestha P, Yang B, Chen Y, Liu S, Maarouf M, Chen JL (2021) Acute infection of viral pathogens and their innate immune escape. *Front Microbiol* 12: 672026

- Rebendenne A, Valadão ALC, Tauziet M, Maarifi G, Bonaventure B, McKellar J, Planès R, Nisole S, Arnaud-Arnould M, Moncorgé O *et al* (2021) SARS-CoV-2 triggers an MDA-5-dependent interferon response which is unable to control replication in lung epithelial cells. *J Virol* 95: e02415-20
- Renk H, Dulovic A, Seidel A, Becker M, Fabricius D, Zernickel M, Junker D, Groß R, Müller J, Hilger A *et al* (2022) Robust and durable serological response following pediatric SARS-CoV-2 infection. *Nat Commun* 13: 128
- Sampaio NG, Chauveau L, Hertzog J, Bridgeman A, Fowler G, Moonen JP, Dupont M, Russell RA, Noerenberg M, Rehwinkel J (2021) The RNA sensor MDAS detects SARS-CoV-2 infection. *Sci Rep* 11: 13638
- Sanjana NE, Shalem O, Zhang F (2014) Improved vectors and genome-wide libraries for CRISPR screening. *Nat Methods* 11: 783–784
- Shaw AC, Goldstein DR, Montgomery RR (2013) Age-dependent dysregulation of innate immunity. *Nat Rev Immunol* 13: 875–887
- Shilts J, Severin Y, Galaway F, Müller-Sienerth N, Chong Z-S, Pritchard S, Teichmann S, Vento-Tormo R, Snijder B, Wright GJ (2022) A physical wiring diagram for the human immune system. *Nature* 608: 397–404
- Sposito B, Broggi A, Pandolfi L, Crotta S, Clementi N, Ferrarese R, Sisti S, Criscuolo E, Spreafico R, Long JM *et al* (2021) The interferon landscape along the respiratory tract impacts the severity of COVID-19. *Cell* 184: 4953–4968
- Stanifer ML, Kee C, Cortese M, Zumaran CM, Triana S, Mukenhirn M, Krausslich HG, Alexandrov T, Bartenschlager R, Boulant S (2020) Critical role of type III interferon in controlling SARS-CoV-2 infection in human intestinal epithelial cells. *Cell Rep* 32: 107863
- Stich M, Elling R, Renk H, Janda A, Garbade SF, Müller B, Kräusslich HG, Fabricius D, Zernickel M, Meissner P *et al* (2021) Transmission of severe acute respiratory syndrome coronavirus 2 in households with children, Southwest Germany, May–August 2020. *Emerg Infect Dis* 27: 3009–3019
- Thorne LG, Reuschl AK, Zuliani-Alvarez L, Whelan MVX, Turner J, Noursadeghi M, Jolly C, Towers GJ (2021) SARS-CoV-2 sensing by RIG-I and MDAS links epithelial infection to macrophage inflammation. *EMBO J* 40: e107826
- Thorne LG, Bouhaddou M, Reuschl AK, Zuliani-Alvarez L, Polacco B, Pelin A, Batra J, Whelan MVX, Hosmillo M, Fossati A *et al* (2022) Evolution of enhanced innate immune evasion by SARS-CoV-2. *Nature* 602: 487–495
- Toh ZQ, Anderson J, Mazarakis N, Neeland M, Higgins RA, Rautenbacher K, Dohle K, Nguyen J, Overmars I, Donato C *et al* (2022) Comparison of seroconversion in children and adults with mild COVID-19. *JAMA Netw Open* 5: e221313
- Urban C, Welsch H, Heine K, Wüst S, Haas DA, Dächert C, Pandey A, Pichlmair A, Binder M (2020) Persistent innate immune stimulation results in IRF3-mediated but caspase-independent cytostasis. *Viruses* 12: 635
- Vanderheiden A, Ralfs P, Chirkova T, Upadhyay AA, Zimmerman MG, Bedoya S, Aoued H, Tharp GM, Pellegrini KL, Manfredi C *et al* (2020) Type I and type III interferons restrict SARS-CoV-2 infection of human airway epithelial cultures. *J Virol* 94: e00985-20
- Venet M, Sa Ribeiro M, Décembre E, Bellomo A, Joshi G, Villard M, Cluet D, Perret M, Pescamona R, Paidassi H *et al* (2021) Severe COVID-19 patients have impaired plasmacytoid dendritic cell-mediated control of SARS-CoV-2-infected cells. *medRxiv* <https://doi.org/10.1101/2021.09.01.21262969> [PREPRINT]
- Venkatesh D, Hernandez T, Rosetti F, Batal I, Cullere X, Lusinskas FW, Zhang Y, Stavrakis G, Garcia-Cardena G, Horwitz BH *et al* (2013) Endothelial TNF receptor 2 induces IRF1 transcription factor-dependent interferon-beta autocrine signaling to promote monocyte recruitment. *Immunity* 38: 1025–1037
- Vono M, Huttner A, Lemeille S, Martinez-Murillo P, Meyer B, Baggio S, Sharma S, Thiriard A, Marchant A, Godeke GJ *et al* (2021) Robust innate responses to SARS-CoV-2 in children resolve faster than in adults without compromising adaptive immunity. *Cell Rep* 37: 109773
- Wang H, Paulson KR, Pease SA, Watson S, Comfort H, Zheng P, Aravkin AY, Bisignano C, Barber RM, Alam T *et al* (2022) Estimating excess mortality due to the COVID-19 pandemic: a systematic analysis of COVID-19-related mortality, 2020–21. *Lancet* 399: 1513–1536
- Whitley RJ, Monto AS (2006) Prevention and treatment of influenza in high-risk groups: children, pregnant women, immunocompromised hosts, and nursing home residents. *J Infect Dis* 194: S133–S138
- Willemsen J, Wicht O, Wolanski JC, Baur N, Bastian S, Haas DA, Matula P, Knapp B, Meyniel-Schicklin L, Wang C *et al* (2017) Phosphorylation-dependent feedback inhibition of RIG-I by DAPK1 identified by kinome-wide siRNA screening. *Mol Cell* 65: 403–415
- Willemsen J, Neuhoft MT, Hoyler T, Noir E, Tessier C, Sarret S, Thorsen TN, Littlewood-Evans A, Zhang J, Hasan M *et al* (2021) TNF leads to mtDNA release and cGAS/STING-dependent interferon responses that support inflammatory arthritis. *Cell Rep* 37: 109977
- Wong LR, Perlman S (2022) Immune dysregulation and immunopathology induced by SARS-CoV-2 and related coronaviruses - are we our own worst enemy? *Nat Rev Immunol* 22: 47–56
- Wu X, Dao Thi VL, Huang Y, Billerbeck E, Saha D, Hoffmann HH, Wang Y, Silva LAV, Sarbanes S, Sun T *et al* (2018) Intrinsic immunity shapes viral resistance of stem cells. *Cell* 172: 423–438
- Wüst S, Schad P, Burkart S, Binder M (2021) Comparative analysis of six IRF family members in alveolar epithelial cell-intrinsic antiviral responses. *Cells* 10: 2600
- Yamada T, Sato S, Sotoyama Y, Orba Y, Sawa H, Yamauchi H, Sasaki M, Takaoka A (2021) RIG-I triggers a signaling-abortive anti-SARS-CoV-2 defense in human lung cells. *Nat Immunol* 22: 820–828
- Yarilina A, Park-Min KH, Antoniv T, Hu X, Ivashkiv LB (2008) TNF activates an IRF1-dependent autocrine loop leading to sustained expression of chemokines and STAT1-dependent type I interferon-response genes. *Nat Immunol* 9: 378–387
- Yin X, Riva L, Pu Y, Martin-Sancho L, Kanamune J, Yamamoto Y, Sakai K, Gotoh S, Miorin L, De Jesus PD *et al* (2021) MDAS governs the innate immune response to SARS-CoV-2 in lung epithelial cells. *Cell Rep* 34: 108628
- Yoshida M, Worlock KB, Huang N, Lindeboom RG, Butler CR, Kumasaka N, Dominguez Conde C, Mamanova L, Bolt L, Richardson L *et al* (2022) Local and systemic responses to SARS-CoV-2 infection in children and adults. *Nature* 602: 321–327
- Zhang Q, Bastard P, Liu Z, Le Pen J, Moncada-Velez M, Chen J, Ogishi M, Sabli IKD, Hodeib S, Korol C *et al* (2020) Inborn errors of type I IFN immunity in patients with life-threatening COVID-19. *Science* 370: eabd4570
- Zhou F, Yu T, Du R, Fan G, Liu Y, Liu Z, Xiang J, Wang Y, Song B, Gu X *et al* (2020) Clinical course and risk factors for mortality of adult inpatients with COVID-19 in Wuhan, China: a retrospective cohort study. *Lancet* 395: 1054–1062



**License:** This is an open access article under the terms of the [Creative Commons Attribution-NonCommercial-NoDerivs](https://creativecommons.org/licenses/by-nc-nd/4.0/) License, which permits use and distribution in any medium, provided the original work is properly cited, the use is non-commercial and no modifications or adaptations are made.